Journal of Nuclear Materials 559 (2022) 153431

Contents lists available at ScienceDirect

Journal of Nuclear Materials

journal homepage: www.elsevier.com/locate/jnucmat

Review

High temperature zirconium alloys for fusion energy

D.J.M. King [a,b,*], A.J. Knowles [a,b,c], D. Bowden [a], M.R. Wenman [b], S. Capp [a], M. Gorley [a], J. Shimwell [a], L. Packer [a], M.R. Gilbert [a], A. Harte [a]

[a] United Kingdom Atomic Energy Authority (UKAEA), Culham Science Centre, Abingdon OX14 3DB, United Kingdom
[b] Centre for Nuclear Engineering, Imperial College London, South Kensington, London SW7 2AZ, United Kingdom
[c] School of Metallurgy and Materials, University of Birmingham, Birmingham, Northern Ireland, United Kingdom

ARTICLE INFO

Article history:
Received 9 June 2021
Revised 4 October 2021
Accepted 22 November 2021
Available online 2 December 2021

Keywords:
Zirconium alloys
Tritium breeder
High temperature materials

ABSTRACT

This review considers current Zr alloys and opportunities for advanced zirconium alloys to meet the demands of a structural material in fusion reactors. Zr based materials in the breeder blanket offer the potential to increase the tritium breeding ratio above that of Fe, Si and V based materials. Current commercial Zr alloys might be considered as a material in water-cooled breeder blanket designs, due to the similar operating temperature to fission power plants. For breeder blankets designed to operate at higher temperatures, current commercial Zr alloys will not meet the high temperature strength and thermal creep requirements. Hence, Zr alloys with an operational temperature capability beyond that of current commercial fission alloys have been reviewed, specifically: binary Zr alloy systems Zr-Al, Zr-Be, Zr-Cr, Zr-Nb Zr-Ti, Zr-Si, Zr-Sn, Zr-V and Zr-W; as well as higher order Zr alloys Zr-Mo-Ti, Zr-Nb-Ti, Zr-Ti-Al-V and Zr-Mo-Sn. It is concluded that, with further work, higher order Zr alloys could achieve the required high temperature strength, alongside ductility, while maintaining a low thermal neutron cross-section. However, there is limited data and uncertainty regarding the structural performance and microstructural stability of the majority of advanced Zr alloys for temperatures 500–700 °C, at which they would be expected to operate for helium- and liquid metal-cooled breeder blanket designs.

Crown Copyright © 2021 Published by Elsevier B.V.
This is an open access article under the CC BY license (http://creativecommons.org/licenses/by/4.0/)

1. Introduction

Materials selection and development for fusion reactors is a primary research topic underpinning the progression of fusion technology. Popular candidates for the structural material in the breeder blanket are Fe, V, Cr, or Si based materials. However, recent work has shown that Zr can offer an advantage over these candidates if used as the structural material within the first wall (FW) of a DEMO-like reactor, where it was predicted to yield a positive tritium breeding ratio (TBR) relative to an omission of a FW material [1]. This may offer particularly important advantages for spherical tokamak reactor designs [2,3], where the reduced volume for breeding would mean a higher TBR is harder to obtain.

The development of Zr alloys for in-core nuclear fission applications began ~60 years ago, as a replacement for steel components. Today, examples of Zr alloys that are in regular use include: Zircaloy-2, −4, ZIRLO™, M5®, Zr-2.5 and E110, for fuel assemblies and fuel claddings in light water reactors. Their success is largely due to the small thermal neutron absorption cross-section (σ_{abs}) of Zr, 0.185 barns (bn), relative to the majority of elements in other structural materials, which allows for a higher availability of neutrons at thermal energies to sustain criticality of the fission reaction. If other materials with higher σ_{abs} are used within the reactor core, the ^{235}U content in the UO_2 fuel must be enriched further, which is generally a more financially costly option.

Fusion energy devices, e.g., International Thermonuclear Experimental Reactor (ITER) [4], Demonstration reactor (DEMO) [4,5], and Spherical Tokomak for Energy Production (STEP) [6], present analogous neutron efficiency challenges to fission. To sustain long-term operation, the tritium (T or ${}^{3}_{1}H$) available for fusion must be replenished. This is to be achieved through the breeding of T during operation via the inelastic scattering of the neutrons produced by the deuterium-tritium (D-T) fusion reaction, with Li, through the following reactions:

$$ {}^{1}_{0}n + {}^{6}_{3}Li \rightarrow {}^{3}_{1}H + {}^{4}_{2}He \quad (1) $$

$$ {}^{1}_{0}n + {}^{7}_{3}Li \rightarrow {}^{3}_{1}H + {}^{4}_{2}He + {}^{1}_{0}n \quad (2) $$

Similar to the fission cross-section of ^{235}U, the T breeding cross-section (σ_T) of the ${}^{6}_{3}Li$ isotope generally increases with decreas-

* Corresponding author at: United Kingdom Atomic Energy Authority (UKAEA), Culham Science Centre, Abingdon OX14 3DB, United Kingdom.
E-mail address: daniel.miks@live.com (D.J.M. King).

https://doi.org/10.1016/j.jnucmat.2021.153431
0022-3115/Crown Copyright © 2021 Published by Elsevier B.V. This is an open access article under the CC BY license (http://creativecommons.org/licenses/by/4.0/)

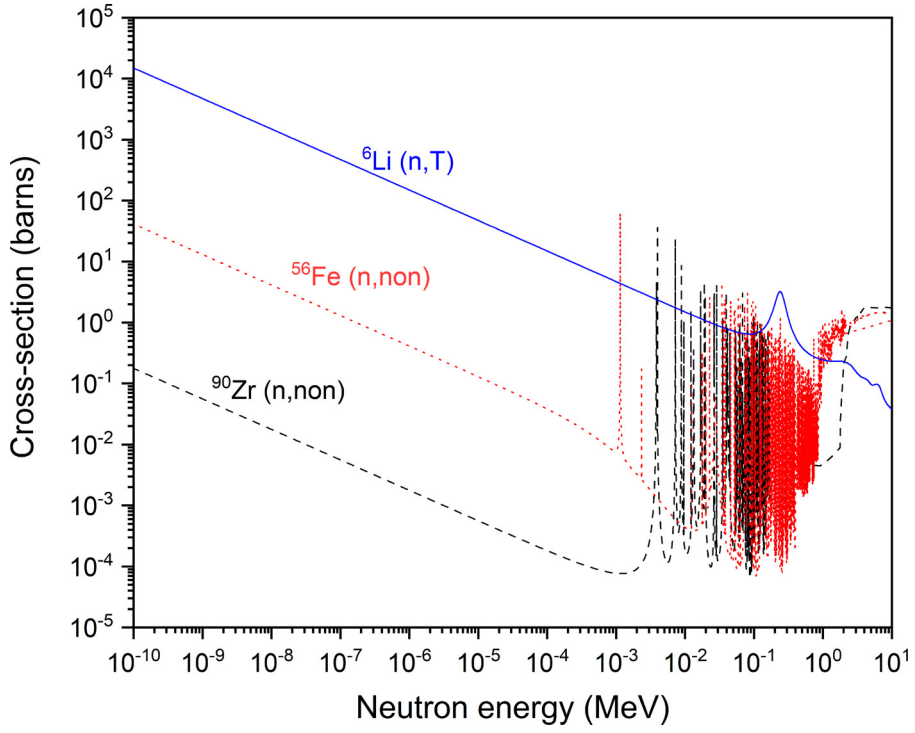

Fig. 1. Neutron cross-section for ^{6}Li breeding T (blue solid line), ^{56}Fe non-elastic scattering (red dotted line), ^{90}Zr non-elastic scattering (black dashed line). Data and references used to contruct figure can be found in Ref. [8]. (For interpretation of the references to color in this figure, the reader is referred to the web version of this article.)

ing neutron energy (proportional to $\frac{1}{\sqrt{Energy}}$) and is exothermic, whereas σ_{T} of the $^{7}_{3}Li$ is a threshold reaction taking place when neutrons energies are above ~2 MeV. Nevertheless, reaction (2) produces T and $^{1}_{0}n$, which is potentially available for further reaction with $^{6}_{3}Li$. Whilst T is produced via both of these reactions in a breeder blanket (the proportion varies depending on the blanket concept), the likelihood of reaction (1) occurring is greater than (2) due to the moderation of neutrons that occurs via elastic scattering with the various components within the reactor (structural material, coolant, multiplier, and reflector) [7]. To exploit these circumstances, enrichment of $^{6}_{3}Li$ is planned for a majority of designs. However, use of a low thermal neutron absorption cross-section material could be used to the same effect and lead to lower costs and greater design freedom for T breeding in the low energy regime (< 1 MeV).

Fig. 1 shows the microscopic neutron cross-sections of T production (n, T) for $^{6}_{3}Li$, and non-elastic scattering (n, non) of ^{56}Fe and ^{90}Zr. It can be seen that both ^{90}Zr and ^{56}Fe exhibit similar resonance behaviour between 1×10^{-2} – 1 MeV but below this range, the cross-section of Zr is significantly lower.

There is a range of proposed designs for future fusion reactors, therefore we must consider a range of conditions that a structural material in the breeder-blanket could be exposed to [5,9]. Some water-cooled fusion reactor designs operate in temperature ranges similar to current light water reactors (300–350 °C [10]), and others operate in a higher temperature regime for improved plant thermal efficiency, where leading designs have coolant outlet temperatures in the region of 500–700 °C [5,9]. Commonly proposed high temperature coolants are: He or H gas, liquid metals such as Li, or molten salts, which will be in direct contact with the coolant pipes composed of the structural material. The structural material will also be in contact with the armour material (e.g. W), the breeder and multiplier material, which are typically Li, Be and/or Pb containing compounds [5,9]. Such alloys will also be exposed to a neutron flux with maximum energies of ~14 MeV [11]. Finally, the mode of operation could be a pulsed mode operation with ~2 h durations and ~5×10^{4} cycles or quasi-continuous [12].

Of the current designs for the test blanket module (TBM) programme on ITER [13,14], the water-cooled lithium lead (WCLL) breeder blanket concept would employ a temperature range most similar to those of current fission power plants (280–325 °C). At these water-cooled operating temperatures in fission power plants, Zr alloys can feature as the fuel cladding, pressure tubes, fuel channels and fuel spacer grids. The helium-cooled pebble bed (HCPB) breeder blanket concept operates at a higher temperature (300–500 °C) and is another most promising TBM design [15]. It has been shown that Zr as a FW structural material would improve the TBR in this a detached FW version of the HCPB concept, with excellent mechanical compatibility between the Zr and W as the plasma-facing material due to their similar coefficient of thermal expansion [1]. However, the mechanical behaviour of current commercial Zr at these higher temperatures would likely be unacceptable. Hence, it is pertinent to review novel Zr alloys for higher temperature mechanical stability and highlight key areas for development.

So-far, there has not been any considerable work towards the development of Zr alloys tailored for fusion, and the primary research direction for Zr alloy development has been towards extended operational life in the environment of a light water fission reactor, *viz.* submersion in an aqueous solution at ~300 °C [16]. Comprehensive reviews on the effects that neutron radiation has on commercial Zr alloys, in fission reactor conditions, can be found elsewhere [17–20] and will not be discussed in detail here. However, it must be noted that dimensional change via irradiation-induced creep and growth will be a concern for the WCLL design. In fission fuel cladding and pressure tubes, strong texture is created during component fabrication to prevent radial hydrogen-induced cracking. This strong crystallographic anisotropy induces highly directional irradiation-induced growth strains, which is a

Table 1
Example compositions (wt.%) of commercial Zr alloys.

Alloy	Sn	Fe	Cr	Ni	Nb	O	Refs.
Zircaloy-1	2.50	–	–	–	–	–	[27]
Zircaloy-2	1.50	0.10	0.10	0.08	–	0.14[b]	[28]
Zircaloy-3	0.25	0.25	–	–	–		[29]
Zircaloy-4	1.50	0.20	0.10	–	–	0.11[b]	[28]
E110	–	0.05	0.02	0.02	1.10	0.10	[30]
Valloy	–	0.10	1.15	–	–		[31]
Ozhenite	0.20	0.10	–	0.10	0.10		[32]
Zr-2.5Nb	–	–	–	–	2.50	0.13[c]	[28]
M5®	0.01	0.05	0.02	–	1.00	0.12	[33]
ZIRLO™	1.00	0.01	–	–	1.00	0.13	[33]
Optimized ZIRLO™	0.67	0.10	–	–	1.00	0.13	[34]

lifetime-limiting effect. Irradiation-induced growth can be completely absent to very high fluences (> 55 dpa) by quenching to the α-phase directly from the β-phase and hence randomising the texture, e.g. see Section 3.4.1 in Ref. [20]. Texture randomisation could therefore be considered as a method to limit anisotropic irradiation-induced dimensional change for Zr alloys in the WCLL breeder blanket design. For the HCPB design, at operational temperatures >500 °C, the predominant dimensional change will not be irradiation-induced creep or growth but simply thermal creep [21]. However, it should be noted that the effects of fusion-relevant higher energy flux profiles at these higher temperatures on irradiation-induced dimensional changes have not been investigated for Zr alloys and the mechanical loading of structural components in the FW blanket (estimated by Forty and Karditas for a Zr alloy previously [22]) will differ to that of a fuel cladding or assembly [23]. While Forty and Karditas concluded that thermal and irradiation creep would not be life-limiting for a Zr-based water-cooled breeder blanket, no such thermo-mechanical analysis has been performed for a helium-cooled design; commercial Zr alloys experience unacceptably high creep rates ($>10^{-5}$ h^{-1}) [21] above 500 °C, wherein lies part of the reason for their lack of consideration for fusion. Of further concern is the susceptibility of Zr to H embrittlement. In a review of this latter topic, Forty and Karditsas [24] concluded that H embrittlement of Zr is unlikely to be a life-limiting factor in a fusion environment. However, more work needs to be done to consider the varying sources of H under non-ideal conditions and the effect of pulsed temperature profile of the reactor on delayed hydride cracking. Nevertheless, given the neutronic advantage of Zr, established world-wide extraction/production routes, and their success in fission environments, some consideration should be made for Zr alloys as a structural material in the breeder blanket.

It is therefore the purpose of this review article to consider the high temperature mechanical properties of current Zr alloys and identify the capabilities of advanced Zr alloys, as well as their suitability as structural materials in a fusion environment. Comparisons are made to other current candidate structural materials: EUROFER 97, V-4Cr-4Ti and silicon carbon fibre/silicon carbide composite (SiC_f/SiC).

2. Current Zr alloys

2.1. Material properties

Currently, ~85% of the globally produced Zr metal is used for nuclear applications (estimated at 6000 t in 2014 [25]). However, this is only a small fraction (<5%) of the total Zr ore extracted annually (~10^6 t), which is used in construction, medical and electronic applications [26]. Natural Zr contains ~4% Hf, which must be removed for nuclear applications due to the high thermal σ_{abs} of Hf (104.1 bn). Across North America and Europe, nuclear grade Zr is processed by three companies: Companie European Zirconium Ugine Sandvik, Allegheny Technologies Incorporated, and Western Zirconium. Strip/sheet and tube manufacturing knowledge and capabilities exist globally e.g. at Westinghouse, Framatome, and Sandvik Special Metal. It is therefore plausible that the world supply of Zr could be upscaled for use in commercial fusion reactors and therefore benefit from the pre-established nuclear supply chain, a feature only Fe alloys currently match.

Table 1 lists example compositions of some popular Zr alloys that have been developed for fission applications. Of these alloys, Zircaloy-2 and −4 have seen the most prevalent use, while M5®, and ZIRLO™ have been the recent successful developments. The design basis for optimised compositions has largely focussed on gaining superior corrosion resistance and reduced H pick-up in aqueous environments.

Fig. 2 provides a broad comparison of start-of-life thermo-mechanical properties (thermal conductivity, strength, ductility, toughness, fatigue and creep) measured experimentally for example commercial Zr alloys, compared to three other material families considered for use as structural materials in breeder blanket: EUROFER 97, ODS-EUROFER, V-4Cr-4Ti and, SiC_f/SiC. It should be noted that the results presented are from a range of studies with differing sample geometries and treatments, therefore care must be taken when comparing exact values. For the purpose of this review only the trends in the data are plotted to provide ease of comparison. Each datapoint used for these trends can be accessed from Ref. [8]. In general, it can be seen that Zr alloys underperform in high temperature strength, fracture toughness, room temperature fatigue and creep compared to the other materials. However, they have comparatively good ductility and mid-range thermal conductivity.

At room temperature the strength of Zr-2 is similar to V-4Cr-4Ti, but will soften more dramatically with temperature, and is significantly lower than EUROFER 97, ODS EUROFER and SiC_f/SiC), between 200 and 800 °C. In terms of ductility, Zr and V alloys have relatively high uniform tensile elongations between 0 and 800 °C, while SiC_f/SiC, EUROFER 97, and ODS-EUROFER can present brittle behaviour in this temperature range. The toughness of Zr alloys changes dramatically with H, He and O content; the data for Zr-2 presented in Fig 2(d) is quoted to be 20 wppm H, which is a factor of 2 higher than commercially as-received Zr-2 [35]. A trend of increasing ductile-to-brittle transition temperature (DBTT) is observed for increasing H in some cases [36] but the behaviour can also change dramatically depending on hydride morphology [37]. Nevertheless, commercial Zr alloys have a relatively low fracture toughness above room temperature, intrinsic to its crystal structure [38], making it worse than the other candidate alloys. Similarly, the creep and fatigue performances are worse than the other candidates and are prohibitive factors for use of current Zr alloys as structural components in the blanket region, even in the absence of radiation damage. This is because such components will likely

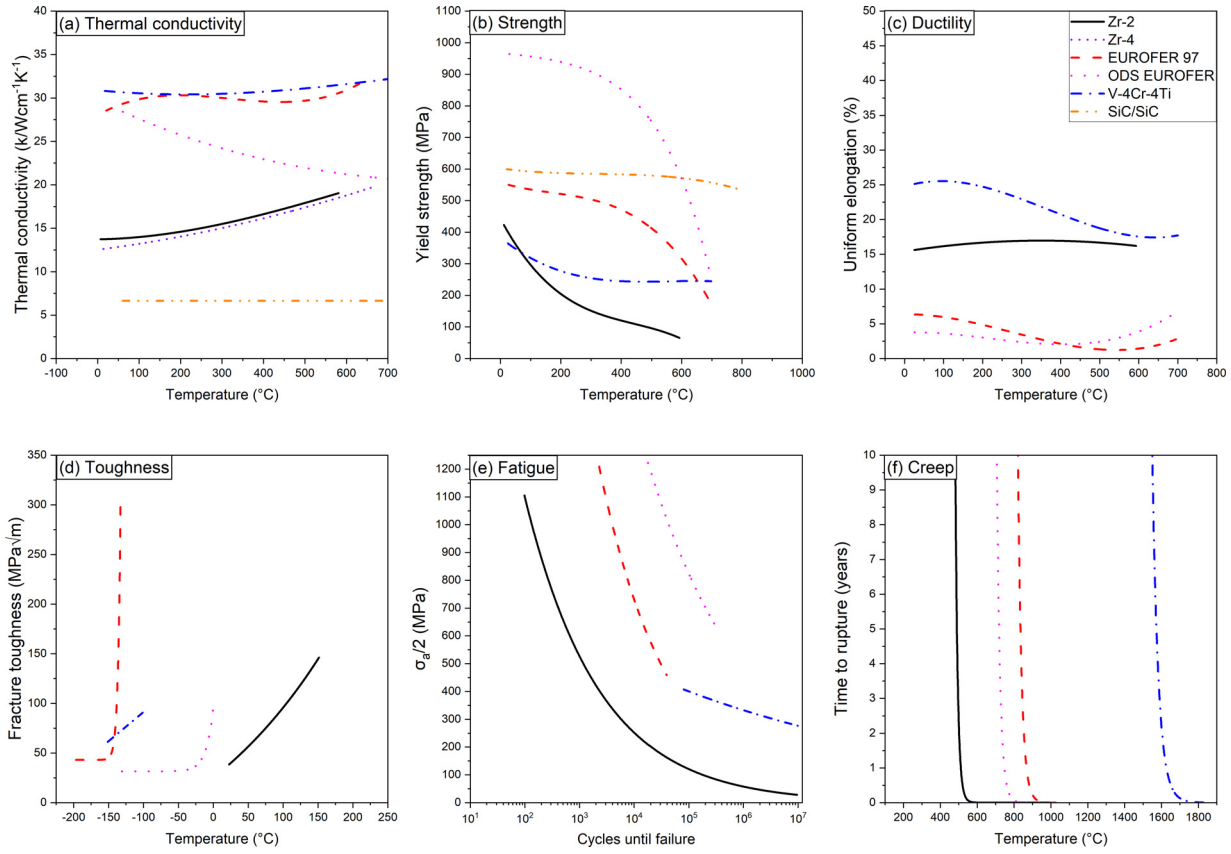

Fig. 2. Relative trends in (a) thermal conductivity, (b) yield strengths (flexural strength for SiC_f/SiC) (c) ductility, (d) toughness, (e) fatigue and (f) creep (50 MPa stress, see Fig. A1), of Zr, V and Fe based alloys and SiC_f/SiC, between 0 and 900 °C. The data and literature references used to construct this Figure are accessible from Ref. [8].

be exposed to cycled thermomechanical loadings, during pulsed mode operation, with maximum operating temperatures higher than the range where commercial Zr alloys can maintain integrity. When including the effects of irradiation, corrosion, cycling, transient conditions, the material design limits become even more restrictive. Previously, EUROFER 97, V-4Cr-4Ti and SiC/SiC have been predicted to have a maximum useful operating temperatures of approximately 550, 650, and 950 °C, respectively, when considering irradiation effects [24]. It is clear that for a Zr based alloy to be suitable as a structural component in the breeder blanket, the creep resistance must be improved. While fatigue and creep data are not available for more novel Zr alloys, here the strength is used as a first order approximation assuming that a stronger alloy will display greater creep resistance.

2.2. Manufacturing, joining, and welding

Currently, components made from nuclear grade Zr are first supplied in the form of sheet, plate or tube. These geometries are then manufactured into the desired shapes or welded to other components.

Allegheny Technologies Incorporated (ATI), for example, produce Zr sponge and Zr alloys in strip, plate, foil and rod geometries [28]. The main difference between Zr alloy components used in fission and fusion are the thicknesses required i.e. more than a magnitude increase in thickness from 0.5 mm of a Zr-4 fuel cladding [39,40]. The use of Zr alloys, when joining and welding for fusion applications, does offer some advantage if a W is to be used as an armour as both elements have similar thermal expansions [41]. However, a well-documented problem resulting from the manufacturing process is the crystallographic texture introduced in the component that leads to anisotropic properties [42], which would persist in conventional Zr alloy components for fusion applications unless a post-manufacture β-quench heat treatment is included for texture randomisation. Atmospheric contamination, at various stages of Zr alloy processing, is also a known problem and therefore vacuums are needed to reduce these effects [43]. It is not expected additional issues relating to the manufacturing, joining and welding of Zr based components, specific to fusion, will be encountered using current methods.

2.3. Effect of impurities (C, H, He, and N)

Impurities can be introduced to a material at all stages of its life. The susceptibility of the material to impurity pickup and the effects of the impurities on mechanical performance is crucial to the viability of the material. It is this aspect that V based alloys face difficulties as C, N and O impurities, introduced during the fabrication process (at concentrations of 60–300, 70–460 and 150–900 wt parts per million [wppm], respectively [44]), lead to loss of workability [45] and weldability [46] and also lead to precipitation during irradiation [47].

The impurity concentrations of Zircaloys, after fabrication, are detailed in Table 2. Within this section, the perceived sources of additional impurity concentrations, material response and possible issues encountered are discussed based on commercial Zr alloys used in a breeder blanket.

2.3.1. Carbon

At high C concentrations (>0.5 wt%) it is known that there is a deleterious effect on the oxidation resistance of Zr alloys. This is because Zr carbides precipitate at the surface and in the bulk of the material and facilitate the diffusion of O into the material

Table 2
Typical start-of-life impurity concentrations in commercial Zr alloys.

Alloy	C (wppm)	H (wppm)	N (wppm)	O (wppm)
Zr-2	270[a]	25[a]	80[a]	1420[b]
Zr-4	270[a]	25[a]	80[a]	1100[b]
Zr-2.5Nb	270[a]	10[a]	65[a]	1300[c]

[a] [28].
[b] [48].
[c] [49].

[50]. At impurity concentrations in Zr-2.5Nb, a correlation between increasing C content between 40 and 300 wppm and deuterium pickup has also been observed [51].

The only other likely source of additional C content in a Zr alloy is in the form of ^{14}C, which can be produced by the interaction of fast neutrons with ^{14}N, via $^{14}N(n,p)^{14}C$. The levels that are produced (~1 wppm/yr [30]) are not expected to have a large impact on the behaviour of the material during operation, but would impact on the induced radioactivity in the material [52].

2.3.2. Hydrogen

Zr has a reasonably large H solubility (>0.15 wt%) at elevated temperatures (>300 °C). Therefore, during thermal cycling there is an energetic drive for H adsorption and dissolution into the metal at high temperatures, and subsequent precipitation as brittle hydride phases at low temperatures where H solubility is very low (~1 wppm at 20 °C). This can lead to hydride re-orientation and the possibility of delayed hydride cracking. These phenomena are well documented for commercial Zr alloys and an extensive review can be found in Refs. [53,54]. The question then shifts to: How much H is available to a structural material in the breeder blanket and what is the H pickup fraction of the material used? In a review by Forty and Karditsas, it is calculated that if the D and T produced by the plasma remains implanted in the armour material, a permeation barrier exists between the breeder and structural material, and there is negligible H pickup from the coolant, then there will be an increase of 27 wppm, due to transmutation, after 5 years of operation [24]. These assumptions are plausible if an effective permeation barrier is developed. Indeed, it was concluded in a review by Davis et al., that at the very least a protective barrier must be in place to prevent the implantation of plasma species to limit H levels in Ti [55]. This notion is further supported by calculations performed by the Japan Atomic Energy Research Institute (JAERI) where it is predicted that for DEMO-like reactors, T permeation from the plasma can be reduced by a factor of 10^3, when the W armour thickness is increased to 1 mm, coated on a low-activation ferritic/martensitic steel, compared to the omission of a FW armour. However, due to the uncertainty in diffusion rates in the various components within the blanket, it is difficult to place an exact T inventory of each component. It is likely that the increased affinity of Zr for H will translate to a higher degree of trapping of T compared to other candidate materials, as seen with V based materials [56]. Further work should be done to assess the T diffusion rate through different materials and observe the T retention in layered systems where barriers between the T sources and a Zr material exist.

2.3.3. Helium

The introduction of He to a Zr alloy will occur due to (n,α) transmutations within the material during operation. Unlike many other materials, He does not lead to excessive void formation and swelling in Zr alloys [57]. It has been predicted in the past, that in a DEMO-like reactor, for a Zr alloy in the blanket region, the He concentrations produced via transmutation will not be a life limiting factor [58]. However, if the alloy is subject to continuous He coolant interaction at elevated temperatures and under neutron irradiation, a different behaviour may be observed. Currently, no data exists that would allow for a reasonable prediction of the surface interaction and oxide behaviour at the coolant interface. Experiments on pure ZrO_2 samples in He environments report some observed changes for temperatures >400 °C using Electron Spin Resonance (ESR) [59]. However, this work is done in the context of catalysis and sensors and does not provide a good indicator of industrial performance for a Zr alloy. Similarly, investigations of He implantation effects at dpas similar to breeder blanket environments have not been conducted, therefore, further experimentation is necessary to investigate whether a He coolant would be compatible with a Zr alloy.

2.3.4. Nitrogen

Historically, N was responsible for increased aqueous corrosion rate in Zircaloys. This effect was counteracted with additions of Sn [27]. However, the Zr manufacturing process has since been refined to reduce the N contents to concentrations that do not substantially impact the corrosion resistance and therefore additional Sn is not needed. As far as the Authors are aware there is no published mechanistic explanations for Sn counteracting the effect of N.

The influence of N on oxidation of Zr alloys has also been documented. The effects have been studied in the context of “loss of coolant accidents” (LOCA) where it has been shown that the presence of N in steam can lead to increased oxidation rate at high temperatures (>600 °C) [60]. The mechanism proposed to be responsible for this, is that nitrides are formed between the oxide and Zr metal interface which accelerates oxidisation of the metal as the nitrides oxidise two orders of magnitude faster compared to a non-nitrided metal [33].

There is not expected to be a significantly high enough concentration of N to be available in the start-of-life Zr or coolant types for deleterious effects to result in a fusion environment.

2.4. Oxidation

When Zr-based alloys are exposed to O, various sub-oxides are formed in a concentration gradient from the metal to ZrO_2 on the surface of the material. The thickness of the ZrO_2 layer will increase with increasing environmental exposure time and temperature [61]. Initially, these oxidation kinetics follow a parabolic or sub-parabolic relationship and have a protective nature. However, this relationship transitions to a linear oxidation rate, termed “breakaway” oxidation, where degradation of the material occurs [62]. Below ~300 °C in air, breakaway oxidation will occur on the order of hundreds of years. However, at temperatures of 600–1000 °C breakaway occurs on the order of hours [63]. At temperatures close to melting, oxidation of Zr in air or steam can lead to catastrophic failures and is a topic of concern for reactor safety [64]. Although fusion reactor breeder blankets will operate in a high vacuum, this rapid failure is of key consideration for accident scenarios and for coolant side exposures; an assessment of the former is made in the following section.

In general, the concentration of impurities, e.g. C, N, H and even O, in the alloy, will increase pre-transition oxidation rate and decrease time to transition [63]. However, the oxidation behaviour is seldom directly proportional with increase in alloying species. Past experimentation on a number of alloying elements (Al, Be, Co, Cu, Cr, Fe, Hf, Mo, Nb, Ni, Pb, Pt, Si, Sn, Ta, Ti, V, and U), in 1, 2 or 4 at.% concentrations, has identified that Be, Ni, and Cu improve oxidation resistance, whereas the others were deleterious or no change was evident to the oxidation behaviour, relative to high purity Zr [63]. However, including elements in lower contents (<1 at.%) often improves the oxidation/corrosion performance [63]. Nevertheless, the oxidation rate of commercial Zr alloys in air and water at mid-range temperatures (~350 °C) have reached a stage in which breakaway is not a concern.

2.5. Corrosion

Aqueous corrosion of conventional Zr alloys is a well-documented process, which involves breakdown of the oxide layer and adsorption/ingress of H. A comprehensive review can be found in Ref. [65]. In short, at temperatures that far exceed nominal fission reactor operation (≥500 °C), aqueous corrosion will be problematic. Therefore, alternative alloys or barrier coatings will need to be utilised in these cases.

For non-aqueous corrosion, the literature is scarce. Regarding liquid metal coolants, Li-Zr alloy interactions have been studied, in the past, as Li is present in the coolant as a pH balance in the form LiOH, in fission reactors. Ingress of Li is known to occur into the Zr oxide layer, which is theorised to increase the porosity and subsequently the corrosion rate [66]. However, the Li-Zr phase diagram predicts complete immiscibility between both species [67], which is supported by the observation that there is no detectable Li concentration in the Zr metal below the oxide layer [66]. It is likely that in a non-aqueous environment, such as if Li or LiPb coolant/breeder is used, that the interaction behaviour with the Zr oxide layer will change significantly. Data of this nature is not available and further work in this area is required.

Much work into liquid metal embrittlement (LME), by corrosion or diffusion controlled intergranular penetration, has been conducted for a range of alloy/metal combinations [68]. However, comprehensive data is lacking for Zr alloy -Li and -Pb combinations. The most relevant work on this topic is likely unpublished and only mentions can be found [69]. Nevertheless, what is mentioned is that Zr based materials are not particularly susceptible to LME by Li with testing being conducted between 482 and 1000 °C [70].

Another aspect that must be considered with exposure of Zr alloys to liquid metal environments is the latter's increased susceptibility to the pickup of impurities. Transfer of material across temperature gradients are typically observed [71], this effect may lead to a heterogenous distribution of impurities within the coolant loop. An assessment of the extent of these effects is needed for Zr alloys and coolants.

In terms of barriers between the structural material/coolant and /breeder, ceramic coatings (e.g. Cr_2O_3) are being developed for both fission [72,73] and fusion applications [74]. It is important to note that if a non-aqueous coolant is used (e.g. Li, PbLi, He, CO_2, FLiBe and FLiNaK), H may still be present as a dissolved impurity or may even be deliberately added as water to improve T extraction. Further, Zr has a high affinity for F and the ZrF_4 formation enthalpy (−4 eV/atom) is significantly more favourable than KF, NaF, LiF, FeF_2 and VF_4 (~−3 eV/atom) [75]. However, Cr has a much lower affinity to F with CrF_6 having a formation enthalpy of −2 eV/atom. Therefore, an effective barrier coating will need to be used regardless of whether aqueous or non-aqueous coolants are used. Moreover, such coatings currently do have promise but further work is still required for industrial applications.

2.6. Accident scenarios

As mentioned, the breakaway oxidation of Zr can lead to catastrophic failure, as evidenced most recently in the Fukushima Daichi accident [76]. This occurs due to the build-up and ignition of H_2 gas resulting from the following reaction:

$$Zr_{(s)} + 2H_2O_{(g)} \rightarrow ZrO_{2(s)} + 2H_{2(g)} \quad (3)$$

For a catastrophic explosive reaction to occur, via this mechanism, three conditions must be met:

- A high volume of H_2O needs to be available for H_2 gas production.
- Sufficiently high temperatures (≥1200 °C [64]) must be reached for rapid oxidation rate.
- Critical gaseous H_2 concentration (15–30 vol.%) in a proportionate layer thickness that allows for flame acceleration and detonation initiation [77].

The reaction rate of Eq. (3) is proportional to the temperature; in the fission industry, emergency core cooling acceptance criteria limits peak Zr cladding temperature to 1200 °C [64]. In the Fukushima accident, the fuel and control rods were completely melted (≥2800 °C) 16 h after loss of coolant occurred. These temperatures are well above the step-change in oxidation rate observed at 1580 °C for Zr [78]. It is thought that approximately 130 kg of H_2 was ignited during the explosion of Fukushima Unit One after ~25 h [79]. Production of this quantity of H_2 would require the reaction of roughly an order of magnitude larger amount of H_2O, which is also roughly 1572 m^3 of water under ambient conditions. The combined volume of the coolant system of ITER is an order of magnitude larger than this [80], therefore if a water coolant is used in a fusion power reactor of similar size, there will be a sufficient supply of H_2O for such volumes of H_2 gas to be produced via oxidation of Zr. However, if a non-aqueous coolant is used, there is not expected to be any other source of H_2O large enough for this to occur.

A large difference between LOCA accidents in fission [81] and fusion [82] environments is that the latter does not have a continued supply of heat generated by the fuel. Therefore, heat will only be generated from the decay of irradiated structural and breeding material. A worst-case LOCA model of a fusion power plant, in which no back-up cooling systems are engaged and minimal heat removal to the environment occurs, predicts that the maximum temperature within reactor will be the FW, which could reach ~1000 °C after 4 days to a maximum of ~1200 °C after 30 days [83]. The latter timeframe is somewhat unrealistic for an accident scenario. However, at these temperatures, the rate of oxidation is on the threshold considered dangerous for Zircaloys [64]. Providing there is a sufficient thermal gradient away from the FW towards a Zr structural material, and/or there is no exposure of Zr to steam at such temperatures, it is not expected that oxidation of Zr will occur at a sufficient rate for H_2 gas accumulation to occur to a sufficient concentration or volume for a catastrophic event to occur during a fusion power plant LOCA.

2.7. Tritium breeding ratio (TBR)

The TBR is the ratio of the rate of T produced during operation Eqs. (1) and (2), to the rate of T burnt in plasma. The feasibility of T breeding depends on both basic physics and engineering issues. It is estimated that a TBR of 1.10–1.15, i.e. incorporating a margin exceeding unity, will need to be achieved to safeguard against periods of breeding losses from decay (time between production and use) and/or incomplete recovery of bred T [84].

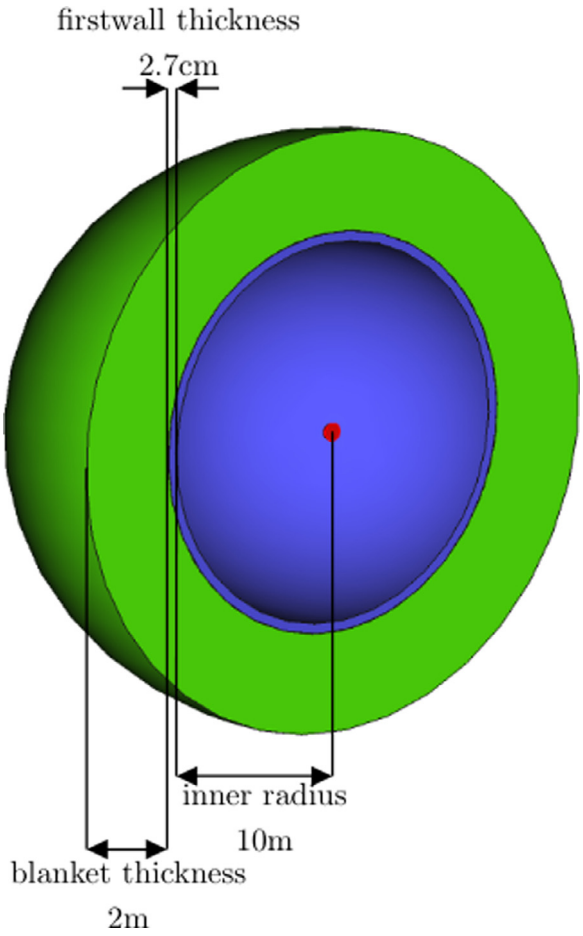

Fig. 3. Cross-section of the simple sphere geometry (not to scale) where the breeder blanket (outer sphere), surrounds the first wall (inner circle) and is separated from the neutron point source (middle circle) by a vacuum.

The TBR when Zr is used as a structural material has previously been calculated by Barrett et al. [1]. In their publication it is stated that the calculations were performed on a He-cooled pebble-bed design, however, details of breeder type, structural fraction, and ^{6}Li enrichment were not provided. Nevertheless, the TBR using Zr, as a structural material in the FW, was calculated to be higher than without a structural material and to be superior to the other candidates (Cr, Fe, V). amongst the other candidates, the relative TBR of V-4Cr-4Ti, ferritic steel and SiC_f/SiC structural materials have been calculated for differing breeders by Sawan and Abdou [84], where it was shown the V-4Cr-4Ti is calculated to achieve the highest TBR of the three candidates, however, Zr alloys were not considered in parallel and there have been no studies that consider the TBR with Zr as a structural material for the whole breeder blanket.

There are many factors that affect the TBR of a fusion reactor, e.g. breeder material, placement, geometry, multiplier, coolant, and ^{6}Li enrichment. As a result, there is a significant range in the calculated TBR when varying these conditions. It is therefore not useful to quote or compare the magnitude of the calculated TBR between different models, and so here we have calculated relative comparisons through a normalised TBR using a simplified system using OpenMC [85], see Fig. 3. The water cooled lithium lead (WCLL) and helium cooled lithium lead (HCLL) designs were simulated to provide a comparison between designs that would operate at temperatures similar to commercial Zr alloys in fission reactors (305 °C) [13,14] and one that operates at higher temperatures (500 °C), respectively. Both designs predicted near identical trends in the data therefore only the results for the HCLL design is shown here. The results for the WCLL design can be seen in Fig. A2 in the *Appendix*. For both, the armour material was W coated EUROFER 97, and Pb-Li as the breeding material. The fraction of structural material (EUROFER 97, SiC, V-4Cr-4Ti, and Zr-4) was varied from 0.0 to 0.9, complimentary to the breeder fraction, which was varied from 1.0 to 0.1, where the TBR at this maximum fraction (i.e. no structural material) is used to normalise the data. The ^{6}Li enrichment fraction in the breeder was also varied from 0.0 to 1.0 and the results are displayed in Fig. 4. Further details of the methodology are provided in the *Appendix*.

From the TBR results in Fig. 3, it is predicted that Zr-4 will outperform all other candidates by up to ~0.1 for structural fractions ≤0.8. Structural fractions above 0.8 are likely far exceeding the structural fractions that are practicable, as current practical designs include EUROFER 97 in the range of 0.14–0.20 material fractions across different breeders [86,87]. Although a TBR increase of 0.1 can certainly be obtained through a variety of methods, such as Li enrichment, redesigning the blanket structure, changing FW thickness, changing coolant etc. Naturally, each method of increasing the TBR will have associated problems. For example increased $^{6}_{3}Li$ enrichment will have associated cost and waste, redesigning the structure to have less structural material could cause weaknesses, increasing the breeder volume will also have increased relative costs compared to the structural material. Further, some reactor designs have less freedoms that influence the TBR than others e.g. spherical reactors do not have room for inboard breeding [88], therefore knowledge of additional methods of attaining an increase in TBR is of interest to the community. This, in addition to the existing industry for mass production and machining of Zr based components, places them at an advantage over other candidate materials. It should be noted, however, that a more focused cost-benefit review of the reactor designs that would most benefit from this increased TBR, using Zr, should be made before committing long-term research efforts into the development of a high temperature Zr structural alloy e.g. reactor designs that are predicted to comfortably meet TBR requirements [89] may not benefit from the use of Zr. Further, designs that utilise Zr alloys complimentary to other candidate materials should also be considered.

2.8. Activation

The activity of the stable elements in the periodic table, 100 years following 2 full power years in a DEMO-like reactor (an approximation of the lifetime exposure of in-vessel components), has been assessed for this review in a similar manner to a previous publication [52]. Each element assessed has been coloured according to their resultant activity in Fig. 5. Of the base elements that constitute the currently considered alloys within this report, the activities of C, Fe, Si and V are within the range of 10^{6}–10^{7} Bq·kg^{-1}, and Zr is more active at ~10^{8} Bq·kg^{-1}. Of the minor metallic alloying elements, Co, Cu, Mo, Nb, Ni and Sn are even higher in activity ranging from 10^{9} to 10^{11} Bq·kg^{-1}. Notwithstanding that Zr is the more active base element, the “cooling” over time is considerably influenced by alloying additions and impurities. For this review, FISPACT-II was used with the same method as Ref. [90] to calculate the activity over time of alloyed examples of the four materials Zr-4, V-4–4, SiC, EUROFER 97, and an armour material W, see Fig. 6. We show that over 100 years the relative activities change considerably. Interestingly, after this time period, it is only SiC, V-4–4, and W that fall below the UK low-level waste (LLW) limit (1.2×10^{7} Bq·kg^{-1}); a design goal pursued by the European fusion research community [91,92]. Nevertheless, Zr-4 presents the highest activity of the candidates. In light of these results, it may be that the activity of such a component cannot meet the aforementioned 100 year LLW goal, while including Zr as a majority element, and that the approach should shift to pursu-

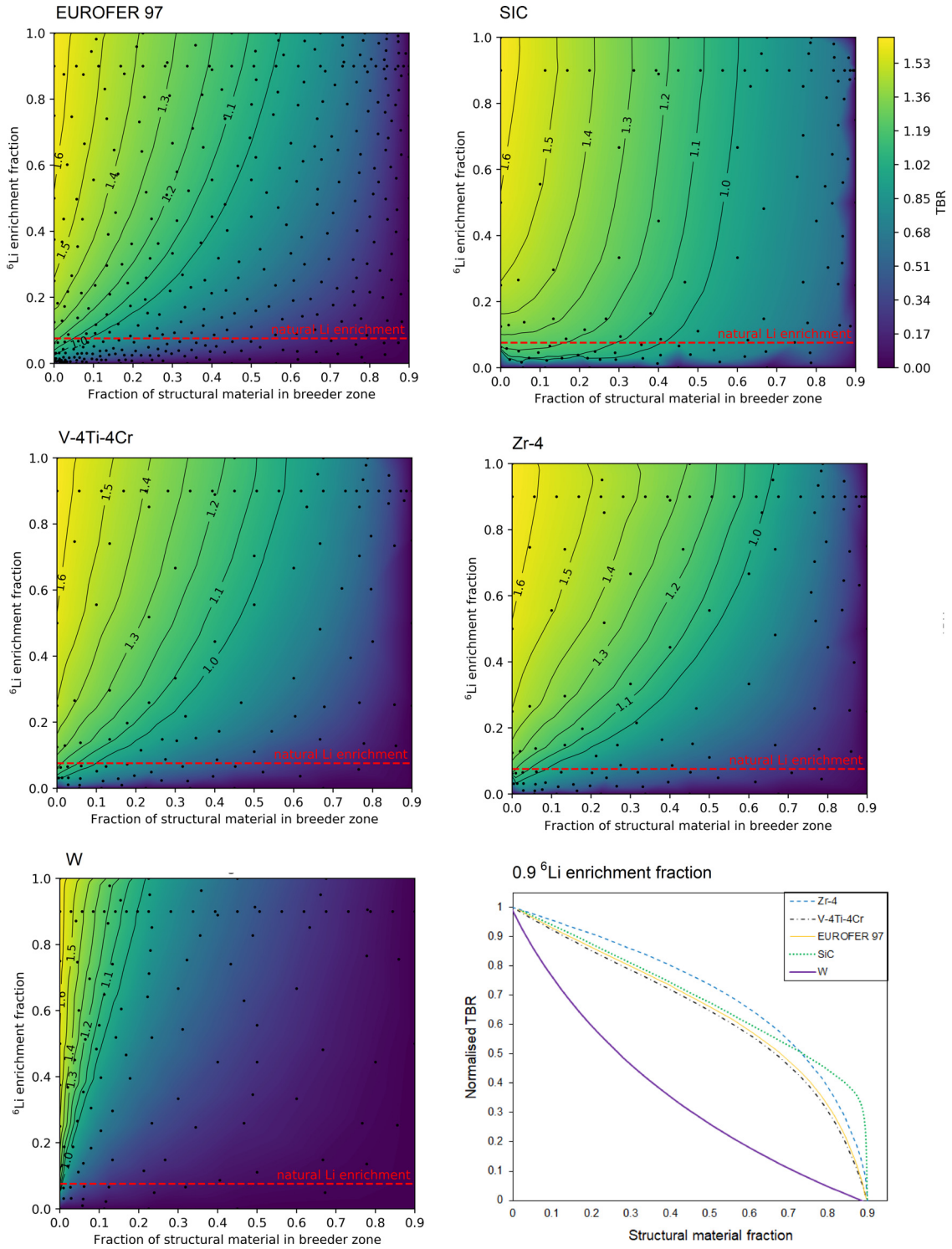

Fig. 4. The tritium breeding ratio (intensity scale and numbered solid lines) of each structural material (labelled panels) calculated at discrete points (solid circles) as a function of structural material fraction and ^{6}Li enrichment fraction. The final panel is a plot of the normalised TBR with 0.9 ^{6}Li enrichment fraction.

ing an "as low as reasonably practicable (ALARP)" [93] design goal. This may be justified via the necessity to achieve a positive TBR in specific reactor designs. However, further cost-benefit analysis is required.

3. Novel Zr alloys

In this section we review opportunities for novel Zr alloys with higher temperature capabilities than conventional Zr alloys, specifically: binary systems of Zr-X, where X refers to elements Al, Be, Cr, Fe, Hf, Mg, Mo, Nb, Ni, Os, Pd, Re, Ru, Sc, Si, Sn, Ta, Ti, V, W and Y, and higher order (3+ element) systems. Microstructure and mechanical property data pertaining to many of these systems is scarce and irradiation data is scarcer. Studies that go beyond that of the initial phase diagram development for non-amorphous Zr rich binary mixtures have been identified and summarised in Table 3. A tally (sum of check boxes) of the type of data is provided as a "score" to quantify the breadth of data available for each sys-

Table 3
Checklist and tally of the type of data identified within this review to be available within the scientific literature for each Zr-X binary system where X is the alloying element. RT, σ and ε refer to room temperature, stress, and strain, respectively.

Alloying element	Microstructure			Mechanical properties			Score	*Pros*	*Cons*	Future work
	As-cast	Heat treated 500–700 °C	Heat treated >700 °C	RT		>RT				
				σ vs ε	Hardness	σ vs ε				
Al	√ [99]	√ [100]	√ [100–102]	√ [100,101,103]	√ [99]	√ [100,101,104]	6	• Low thermal neutron absorption cross-section. • Precipitate and solid solution strengthening. • Good ductility. • Good creep resistance. • Similar level of activity to Zr ($\sim 4 \times 10^8$ Bq·kg^{-1}).	• Lack of ductility when surface flaws are present. Susceptible to corrosion in aqueous environments. •	• Strengthen compositions that are ductile at room temperature (≤7.8 wt.% Al). • Increase ductility of the stronger more creep resistant compositions (>7.8 wt.%). The effect of alloying additional species is the most obvious avenue of exploration.
Nb	√ [105]	√ [106,107]	√ [108]	√ [105,108]		√[109]	5	• Relatively low thermal neutron absorption cross-section. Can present good room temperature strength and ductility due to dual α-(Zr,Nb) + β-(Zr,Nb) phase morphology.	• Between 500 and 700 °C segregation will occur. • Nb has a significantly higher activity (10^{11} Bq·kg^{-1}).	• Addition of Nb in concentrations <2.5 wt.% that dissolve into the α-Zr phase for solid solution strengthening or mixing of other elements that form better precipitate morphologies with Nb.
Sn		√ [110]	√ [110,111]	√ [112]	√ [110]	√ [112]	5	• Low thermal neutron absorption cross-section. Increased creep resistance.	• Inadequate strength as binary alloy for structural applications at 500–700 °C. • Sn has a significantly higher activity ($\sim 2 \times 10^{11}$ Bq·kg^{-1})	• Alloying of additional species is required to achieve higher strengths.
Be	√ [113]	√ [114]	√ [114]	√ [114]			4	• Low thermal neutron absorption cross-section. • The Be_2Zr precipitate is not an embrittling phase and provides good room temperature mechanical properties. • Improves corrosion resistance.	• Toxicity of Be compounds • Low natural abundance • Be has a significantly high activity (9×10^{10} Bq·kg^{-1})	• The mechanical properties at elevated temperatures need to be examined.
Ti	√ [115]		√ [115,116]	√ [115,117]			3	• Allows for tailoring of $\alpha \rightarrow \beta$ transition temperature. • Good room temperature mechanical properties. • lower activation (4×10^6 Bq·kg^{-1})	• Relatively higher thermal neutron absorption cross-section. •	• Investigation of β phase retention during ageing and mechanical properties at elevated temperature.
Cr		√ [118]	√ [118,119]	√ [118,119]			3	• Good precipitate strengthening. • Cr will have a significantly lower activity to Zr (10^6 Bq·kg^{-1}). • Can form stable oxide layer.	• Alloying of Cr limited by higher thermal neutron absorption cross-section.	• Ageing studies and mechanical property experiments are required.
Si	√ [120]		√ [121]	√ [120]			3	• Low thermal neutron absorption cross-section. • Good precipitation strengthening with maintenance of ductility. • Potential for creep resistance. • Lower activity Zr ($\sim 10^7$ Bq·kg^{-1})	• Will likely form additional embrittling silicides when alloyed with other species.	• Theoretical work to predict resultant silicides due to alloying with other species should also be done. • Annealing experiments are needed to determine if the Zr_3Si silicide forms at 500–700 °C. • Mechanical properties at temperature will also need to be evaluated.
Fe	√ [118]	√ [118]	√ [118]				3	• Opportunity for precipitate strengthening. • Lower activity ($\sim 10^7$ Bq·kg^{-1}).	• Fe may segregate and cause embrittlement due to fast diffusion in Zr.	• Ageing studies are required to identify the stability of the Zr_2Fe phase. Annealing studies of polycrystalline Zr-Fe alloys are required to determine resultant microstructures.
Mo	√ [122]	√ [123]				√ [123]	3	• May provide resistance to H retention and corrosion resistance in water. • High melting temperature.	• Higher thermal neutron absorption cross-section. • Low strength at 400 °C. • Significantly higher activity (10^{11} Bq·kg^{-1})	• Microstructural and mechanical property testing with alloying of additional species.
V			√ [124]	√ [124]			2	• Could be used for precipitate strengthening. • V has a lower activity (10^7 Bq·kg^{-1})	• Alloying of V limited by its higher thermal neutron absorption cross-section.	• Examine the microstructures and mechanical properties of components aged between 500 and 700 °C.
W			√ [125]	√ [125]			2	• Very high melting temperature • High strengths • Lower activity (10^7 Bq·kg^{-1})	• Very high thermal neutron absorption cross-section. Difficult to alloy and can produce inhomogeneous, brittle microstructures.	• Investigation of methods that allow for better homogenisation of microstructure e.g. magnetron sputtering, mechanical alloying, or additive manufacturing.
Hf			√ [126]				1			
Os		√ [127]	√ [127]				1			
Ru		√ [128]					1			
Re			√ [129]				1			
Y			√ [130]				1			
Mg							0			
Ni							0			
Pd							0			
Sc							0			
Ta							0			

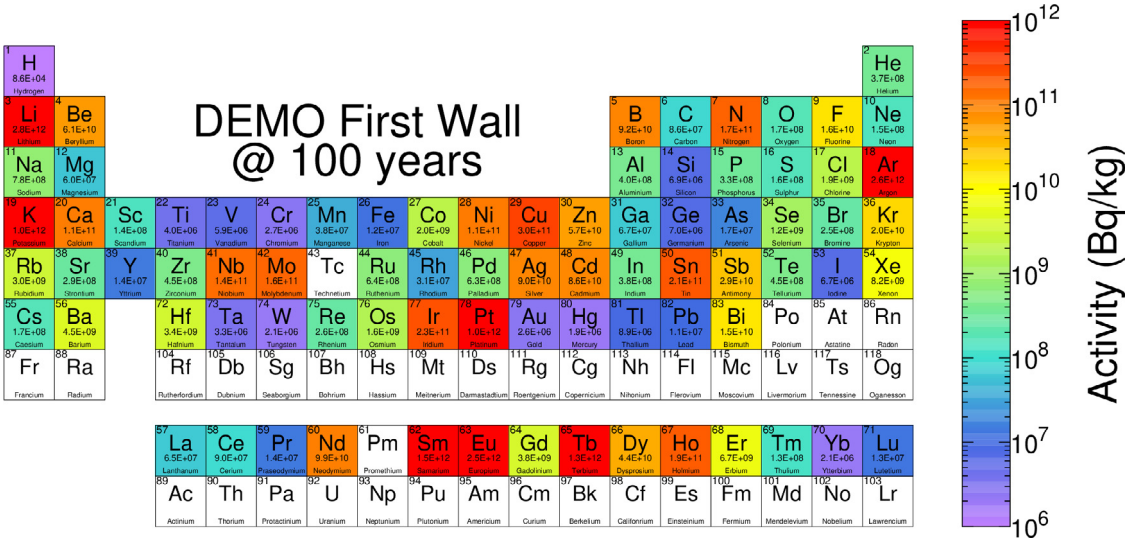

Fig. 5. Periodic table showing the total becquerel activity from each element after 100 years of decay cooling following a 2 full power year irradiation in a DEMO firstwall environment. The colour of each element reflects the activity according to the Bq·kg^{-1} legend, but the absolute values are also given beneath each element symbol.

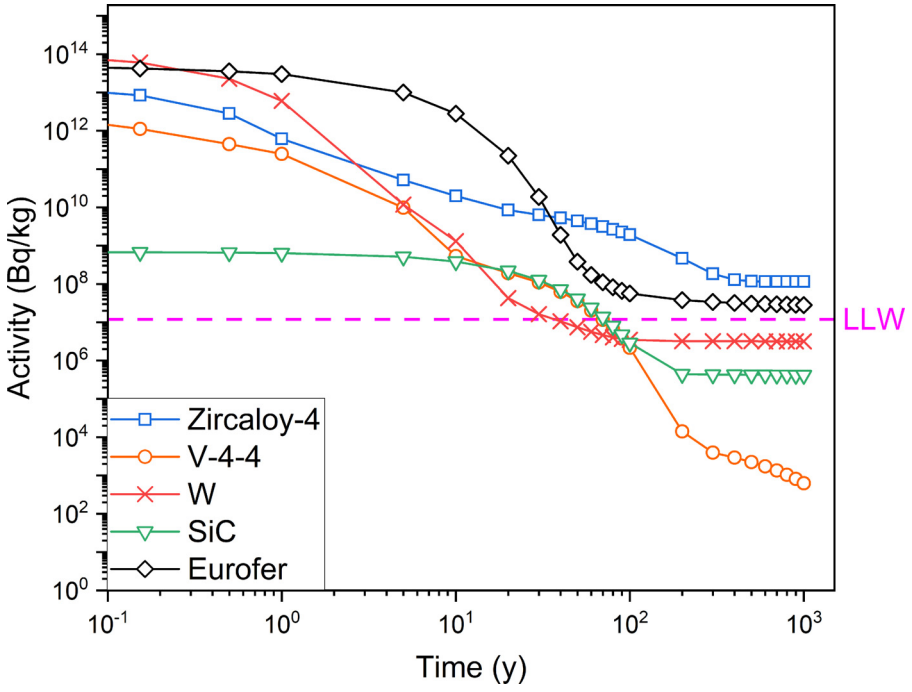

Fig. 6. Activity of Zr-4 (blue squares), V-4–4 (orange circles), W (red crosses), SiC (green triangles) and EUROFER 97 (black diamonds) as a function of time. The UK low level waste limit (LLW) is denoted by a horizontal fuchsia dashed line. (For interpretation of the references to color in this figure, the reader is referred to the web version of this article.)

tem. Systems with scores ≥2, have been discussed in the following subsections.

It is recognised that there are many different breeder designs proposed for DEMO-like fusion reactors. Here we do not provide an assessment for a specific design, rather, we assume the operating temperature ranges from room temperature (RT) to 700 °C to cover a range of designs [94]. Further, work in the context of the Zr alloy to be used as a structural component is reviewed but it is recognised that there are also works that focus on Zr as a T storage material, e.g. Zr61Co39 (wt.%) [95,96], which is not reviewed here. Comments on activity and thermal neutron absorption cross-sections refer to data presented in Fig. 5 and Fig. 7, respectively. Measures of "good" strength and ductility are relative to conventional Zr alloys (~400 MPa), and the minimum uniform elongation of a material to be considered ductile (5%) [97], respectively, at room temperature. Assessments of activity are made from Fig. 5, i.e. 100 years after operation in a DEMO-like reactor and comments are made relative to Zr. Finally, the available mechanical property data, and calculated thermal neutron cross-sections for the specific compositions tested in each system, are compared in the section proceeding the binary and higher order systems.

3.1. Binary Zr systems

3.1.1. Zr-Al

The solubility of Al in Zr is ~1 at.% in the α-phase at temperatures ≤600 °C. The intermetallic compound, Zr_3Al (cubic $L1_2$), exists immediately outside these bounds [131]. The Zr_3Al inter-

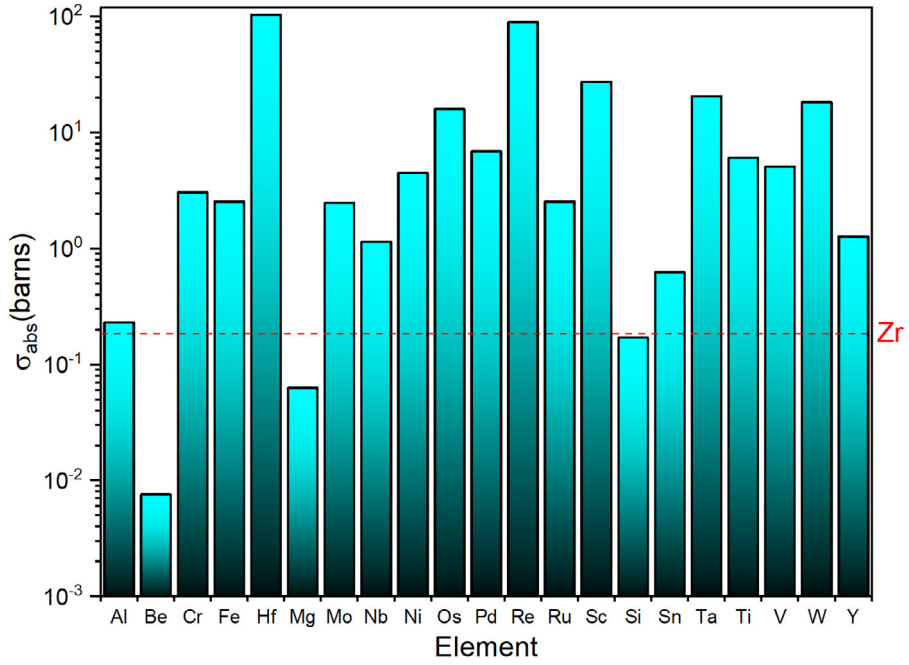

Fig. 7. Microscopic thermal neutron absorption cross-sections (y-axis) of each labelled element (x-axis). Values plotted from Ref. [98] for neutron energies of 2.53×10^{-8} MeV.

metallic is relatively ductile due to the five independent {111}⟨110⟩ slip systems of the $L1_2$ structure [100] and has been demonstrated to exhibit room temperature ductility [103]. A significant body of work on mixtures close to 3Zr:1Al has been performed, pioneered by Schulson in the 1970s, for use as a structural material in nuclear fission reactors [100]. Zr_3Al forms via peritectoid transformation at ~1020 °C between β-Zr and Zr_2Al (tetragonal $B8_2$). Due to the lack of solubility of excess Zr or Al in the compound, monolithic samples have not been studied to date, and instead Zr_2Al and α-Zr are also present in the microstructure, where they are observed at intra and intergranular locations, respectively. The mixing of Al in excess of 7.8 wt.% Al increases the phase fraction of Zr_2Al (>10 vol.%) and decreases the room temperature elongation. Conversely, a deficiency of Al below 7.8 wt.% will decrease the Zr_2Al phase fraction and increase ductility [104]. It is hypothesised that the morphology of the intergranular region, i.e. solid solution of α-(Zr,Al), contributes to the ductility of the material; analogous to the Ni_3Al intermetallic that can be made ductile at room temperature by B doping, which is thought to lead to the formation of a disordered face centred cubic (FCC) phase at the grain boundary [132]. Therefore, in Zr_3Al, a decrease in Al content will also promote grain boundary α-(Zr,Al) formation increasing ductility.

The extent of ductility of this material is highly dependant on the surface state. For example, a polished material with Al concentration of 8.6% can exhibit room temperature elongation of ~30% at failure, however, if stress concentrations such as machining marks or abrasions exist, the total elongation has been measured to be ≤5% [101,133]. This notch sensitivity may be a limiting factor for the use of such a material in a large-scale industrial setting, where surface state is difficult to control. As-such for the purposes of this review, the material is assumed not to be in a polished state.

For long term (≥1000 h) operation at elevated temperatures (500–700 °C) it is possible that grain growth will occur. A study of the mechanical properties as a function of grain size and temperature has been performed for 8.9 wt.% Al samples [103]. After ageing for 1000 h between 800 and 1000 °C, a decrease in room temperature yield strength from ~650 to 180 MPa was measured. This corresponded to grains sizes increasing from 1.6 to 65.0 µm. This extent of softening is likely too severe for the structural requirements in a breeder blanket. However, additional work has shown that some degree of resistance to grain growth can occur between RT and 600 °C where samples maintained grainsize at ~29 µm [100], although the heating rate of the samples was not explicitly stated. This resistance was attributed to the Kear-Wilsdorf type dislocation mechanism, also observed in other $L1_2$ materials [100]. It follows that if resistance to grain coarsening at ageing temperatures between 500 and 700 °C can be demonstrated during long term ageing treatments, it is plausible that this material could meet the strength requirements of a structural material in the breeder blanket.

Irradiations using electrons, light/heavy ions and neutrons have been performed on the Zr_3Al precipitate from RT to 400 °C [134]. It is observed that the structure disorders initially and then amorphises at higher fluences (equivalent of >1.4 dpa) between the aforementioned temperature range. There is an irradiation-induced swelling (≤ 5 vol.%) associated with this disorder but it is inversely proportional to irradiation temperature. Post-irradiation annealing at 575 °C for 1 h allows for a complete recovery of damage [135].

In a study of α-Zr alloys with lower Al concentrations (3–15 at.%) [102], samples were hot-rolled at 920 °C then air cooled. Single-phase α-Zr microstructures were observed until Al was included in concentrations ≤ 9 at.%. Above 9 at.%, precipitation of Zr_3Al occurred. It is assumed that the cooling rate of the samples did not allow for precipitation below <9 at.% Al, an assumption supported by a separate study that observes Zr_3Al precipitation in a 6 at.% sample after annealing for 4 h at 800 °C [136]. Nevertheless, a significant strengthening effect was demonstrated, with a maximum measured yield stress of ~1200 MPa. Furthermore, a good retention of ductility is observed for compositions with ≤12 at.% Al with ~8% total elongation.

The steady state tensile creep rates of compositions close to 3Zr:1Al have been measured at various temperatures and stresses [137]. Fig. 8 provides a comparison between these creep rates and that of EUROFER 97 [138], ZIRLO™ [139], and Zr-2.5Nb [140], extrapolated to applied stresses of 70 MPa, from past experimental data. It should be noted that there are differences in geome-

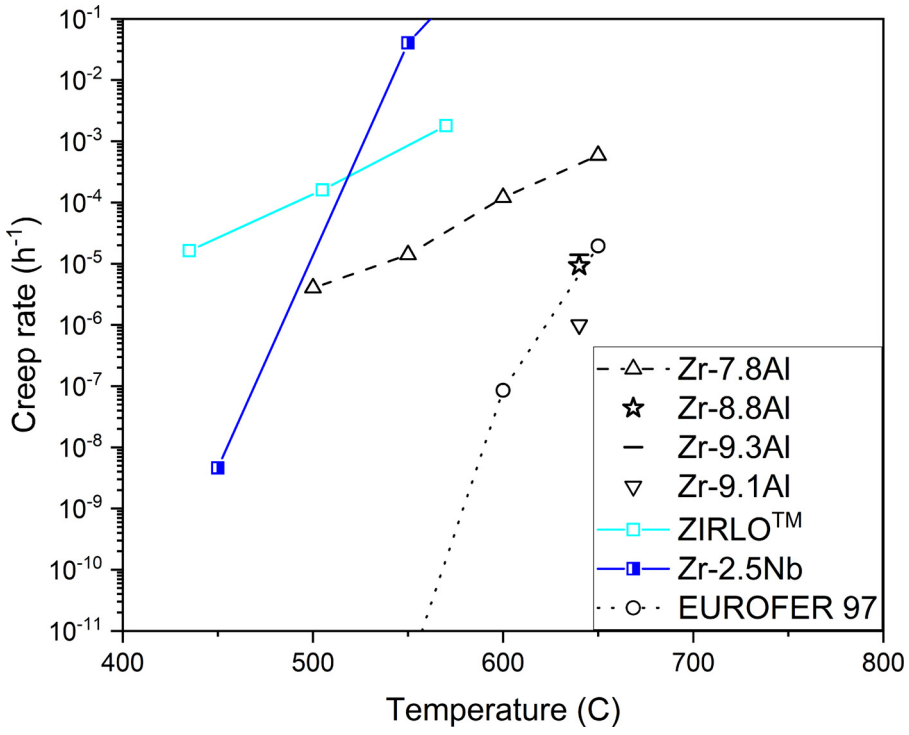

Fig. 8. Thermal creep rate of different Zr-Al compositions (wt.%) compared to ZIRLO^{TM}, Zr-2.5Nb and EUROFER 97 under stresses of 70 MPa.

tries and test conditions between the different studies therefore some error may be associated in the comparisons. Nevertheless, for the Zr-Al compositions with 6.8–7.8 wt.% Al, the reported thermal creep rates an improvement relative to ZIRLO^{TM} and Zr-2.5Nb, and sufficiently low for use at temperatures $\lesssim$550 °C. The thermal creep rate was measured to decrease by an order of magnitude for compositions with 8.5–9.3 wt.% Al and for a sample with 8.8 wt.% Al, a creep rate of 9.3 $\times$ 10^{-6} hr^{-1} was measured for a stress of 70 MPa at 640 °C. Indeed, when Al is included between 8.8 and 9.1 wt.% the creep rate is comparable to EUROFER 97 for temperatures ~650 °C. However, as mentioned previously, there are issues with the ductilities of samples with Al contents in this range, which may be a prohibitive factor for machining of components suitable for a breeder module.

Of additional concern is the susceptibility to corrosion of Zr-Al alloys in aqueous environments [141]; the α-(Zr,Al) phase forms an oxide morphology susceptible to corrosion and an increase in its phase fraction increases the corrosion rate [142]. Therefore, it is likely such materials will be more suited to a breeder blanket that employs non-aqueous coolant. To this end, Al is observed to play a key role in corrosion resistance against Pb coolants through the formation of a Al_2O_3 scale in other alloys [143]. However, Zr has a higher activity with O than Al and is likely to take precedence to form ZrO_2, as observed in the past [144].

3.1.2. Zr-Nb

Niobium is a common alloying addition to Zr in 2.5 wt.% contributions to form the Zr-2.5Nb alloy, which is popularly used in Canadian nuclear power plants [145] and is also under consideration for biomedical applications [146]. The attractiveness of this system is the duplex α-(Zr,Nb) + β-(Zr,Nb) forming region between 615 and 970 °C, which gives rise to a good combination of strength/ductility (~800 MPa/~14% uniform elongation, respectively, at room temperature [145]), grain size and microstructure control, as well as good corrosion/oxidation resistance in light water reactor environments.

For fission applications, Zr-2.5Nb tubes are traditionally extruded at 815 °C, cold-worked 27%, and stress relieved at 400 °C for 24 h. In this state, a metastable network of β-Zr filaments surround elongated grains of α-Zr. Between 400 and 700 °C, the Zr content of the β phase has been observed to reduce with ageing time. The maximum time the Zr rich β-phase was found to be stable was 1000 h [107]. Further, the β-phase will be composed of ~95 wt.% Nb after 10^4 h of ageing, and between 400 and 500 °C ω-Zr (metastable hexagonal [147]) is observed to form within hours of ageing [107].

For operating temperatures between 500 and 700 °C the alloy will be outside of the α(Nb,Zr)+β(Nb,Zr) forming region. Instead, segregation will occur where body centred cubic (BCC) Nb precipitates decorate α-Zr grain boundaries [106,148]. It is therefore not predicted that Zr-2.5Nb will retain its room temperature ductility after long term operation at temperatures relevant to a breeder blanket.

Evaluation of the mechanical properties of Zr-2.5Nb has been conducted between 20 and 1200 °C with a hold time at each temperature of 3–5 min. A sharp decrease in yield strength was observed after 550 °C accompanied by a drastic increase in elongation attributed to the manifestation of superplasticity [109].

M5® is also an example of a commercial Zr-1.0Nb (wt.%) alloy developed for oxidation resistance and reduced H pickup in light water reactors. There is a notable trend in reduction of Sn and retention or increase in O to improve corrosion resistance in commercial Zr alloys [149]. The effect of O content (0.14–4.00 wt.%), in M5® and Zr-4, on the mechanical properties has been observed to stabilise the α phase to higher temperatures but embrittle the alloys at RT, at >0.50 wt.% concentrations [150].

Tensile hoop tests have been performed on M5® cladding irradiated for five and six annual cycles (i.e. fuel burnup of 60–75 $GWd{\cdot}tU^{-1}$) at temperatures between 250 and 800 °C [151]. It was observed that the yield strength of M5® decreased linearly with temperature. M5® also displayed a lower yield strength than Zr-4 between 250 and 600 °C where it decreased from 500 to 200 MPa. However, between 600 and 700 °C the yield strength was quite

similar to Zr-4 (250–150 MPa). The uniform elongation of M5® was recorded to be ~1% between 250 and 450 °C but a lot larger at higher temperatures (4.2–6.4% at 600 °C and 8% at 700 °C) for a high strain rate of 1 s^{-1}. It should be noted that the heating rate of these tests were also quite high (200 °C·s^{-1}) therefore these results are not indicative of samples in their equilibrium microstructures at these temperatures.

It is difficult to translate tensile hoop test results with high strain/heating rates to a prediction of performance of such alloys in a breeder blanket environment. The following points may be applicable:

1 The irradiated mechanical performance of M5® is not markedly different from Zr-4 and likely unsuitable for a breeder blanket material due to high thermal creep rates.
2 The addition of Nb and/or O may be a more interesting avenue to explore for resistance of H pickup.

3.1.3. Zr-Sn

Tin is a common addition to Zircaloys to increase the creep resistance, stabilise α-Zr, and control grain size during processing. However, its addition has been shown to reduce corrosion resistance [152]. It is measured to be soluble in the α-Zr matrix up to 5 at.% at 600 °C. Outside these bounds the phase diagram predicts a cubic Zr_4Sn intermetallic to form, which can exist in an off stoichiometric Zr_3Sn composition [153].

Tin is hypothesised to increase the creep resistance of Zr alloys through mechanisms such as: increase in stress field around Sn (due to the difference in atomic radii) restricting the gliding of dislocations and diffusion of vacancies and lowering of stacking fault energy [154]. Limited studies on pure Zr-Sn binary systems that examine the mechanical properties exist in the open literature, however, various investigations into the microstructure exist [110–112,153]. The tensile properties of β-quenched and tempered martensitic alloys with 2–7 at.% Sn has been investigated [112]. The elongation was not measured to be proportional to Sn content and ranged from 5 to 15% at room temperature. The yield strengths ~250 MPa are seemingly independent of Sn content at room temperature. The microstructural analysis revealed precipitation and unidentified black spots in all samples, which is not predicted from the phase diagram for those with ≤5 at.% Sn. Therefore, these results may not be indicative of the binary systems at equilibrium.

3.1.4. Zr-Be

Beryllium is an element that has been considered for use as a FW material for fusion power reactors due to its low atomic mass, high melting temperature and neutron transparency [155]. It is also a prime candidate for use as a neutron multiplier [156]. Be does not form a solid solution with Zr, instead, it forms a Be_2Zr intermetallic compound below 820 °C [157], which is an ordered hexagonally close packed (HCP) structure [158]. The mechanical properties of mixtures with 2.5 – 9.3 at.% Be have been studied [113]. As anticipated, the microstructure consisted of α-Zr and Be_2Zr at all concentrations, where the latter is observed to form at the grain boundaries, see Fig. 9. A reasonable trade-off between increase in strength (672–892 MPa) and decrease in ductility (14–7% total elongation) was measured over this Be range. Additional experiments were performed on the 5 at.% Be sample where it was hot-rolled and then vacuum annealed at multiple temperatures between 600 and 850 °C for 2 h. A decrease in strength from 786 to 600 MPa, and increase in elongation from 12 to 17% is observed due to the increase in α-Zr recrystallisation fraction, grain size, and decrease in dislocation density [114].

It is worth noting that Be has been identified as one of the few elements that increases the oxidation resistance of pure Zr when alloyed in larger quantities (1, 2 or 4 wt.%) [141].

3.1.5. Zr-Ti

Titanium and Zr are mutually soluble with each other and the $\alpha \rightarrow \beta$ transition temperature is at its lowest (~600 °C) when they are alloyed in equal atomic ratios [159]. A number of studies of binary alloys with 10–50 at.% Ti have been performed, however, these focus on room temperature applications with β phase retention, and the samples are in a quenched state from the β forming region (≥900 °C) [115,117,160,161]. For a structural material operating in the 500–700 °C region, a single β phase is unstable and a high portion α phase will likely transform. One study of a 50 at.% Ti alloy provides results pertaining to samples quenched from 620 to 750 °C [162], which is likely most applicable to a breeder blanket. At room temperature, only α'-phase (β transformed α) was observed, and the room temperature mechanical properties were measured to be 800–1100 MPa ultimate tensile strength (UTS) with 4–7% elongation.

3.1.6. Zr-Cr

Chromium is a common addition in Zircaloys and was initially included as it was found to enhance corrosion resistance and provide strength [16]. However, the solubility of Cr in Zr is very low below ~700 °C where the $ZrCr_2$ C15 Laves phase will form at equilibrium [163]. The C15 Laves phase is a relatively strong but brittle intermetallic compound [164]. $Zr(Cr,Fe)_2$ intermetallics of the same structure are observed to amorphise at RT to 300 °C and dissolve between 300 and 400 °C under neutron irradiation due to radiation enhanced diffusion effects [165].

A study of the mechanical properties of arc melted then hot-rolled (870 °C) Zr with 0.5–3.0 at.% Cr has been performed [119]. Relatively high room temperature strengths were achieved 966–1270 MPa with associated 12.6–6.0% elongation. Further, annealing experiments were carried out on a 1.8 at.% Cr sample at 550, 650 and 750 °C for 1 h, then air cooled [118]. Significant improvements to the ductility were achieved (16–18% from 8.8% elongation) accompanied by decreases in strength (818–991 MPa from 1118 MPa) due to coarsening of grains and reduction in dislocation density.

3.1.7. Zr-Si

Silicon forms a range of complex metallic silicides that are strong but brittle intermetallic phases. Some are widely considered for high temperature structural applications [166], including neutron reflector components in fast reactors [121]. The Zr-Si phase diagram predicts the formation of Zr_3Si, a tetragonal intermetallic, when the temperature and Si concentration is <1571 °C and <15 at.%, respectively [167]. However, a study on an 8.8 at.% mixture did not contain the Zr_3Si phase in the as-cast state [120]. Instead, a tetragonal Zr_2Si intermetallic was formed, evenly dispersed, with sizes ranging from 3 to 10 μm, in the α-Fe matrix, see Fig. 10. The compressive yield strength was measured to be 700 MPa with 13% compression strain to failure at room temperature. Silicon additions to Ti alloys have been shown to improve creep resistance due to their strong pinning of dislocations, and grain/lath boundary sliding [168], therefore, further work into the Zr-Si system is warranted.

3.1.8. Zr-Fe

Iron is a common addition to current Zr alloys due to the strengthening provided by the precipitation of $ZrFe_2$ (C14) and Zr_2Fe (C16 Laves phase) secondary phase particles. In the binary system, Fe has a solubility limit of ~4 at.%, in α-Zr, above 775 °C. Below this temperature, Fe is essentially insoluble and will instead form the Zr_3Fe, an orthorhombic intermetallic, at equilibrium [169]. The diffusion of Fe is relatively fast and segregation to the surface of single crystal samples is observed near instantaneously between temperatures 450–750 °C [170,171].

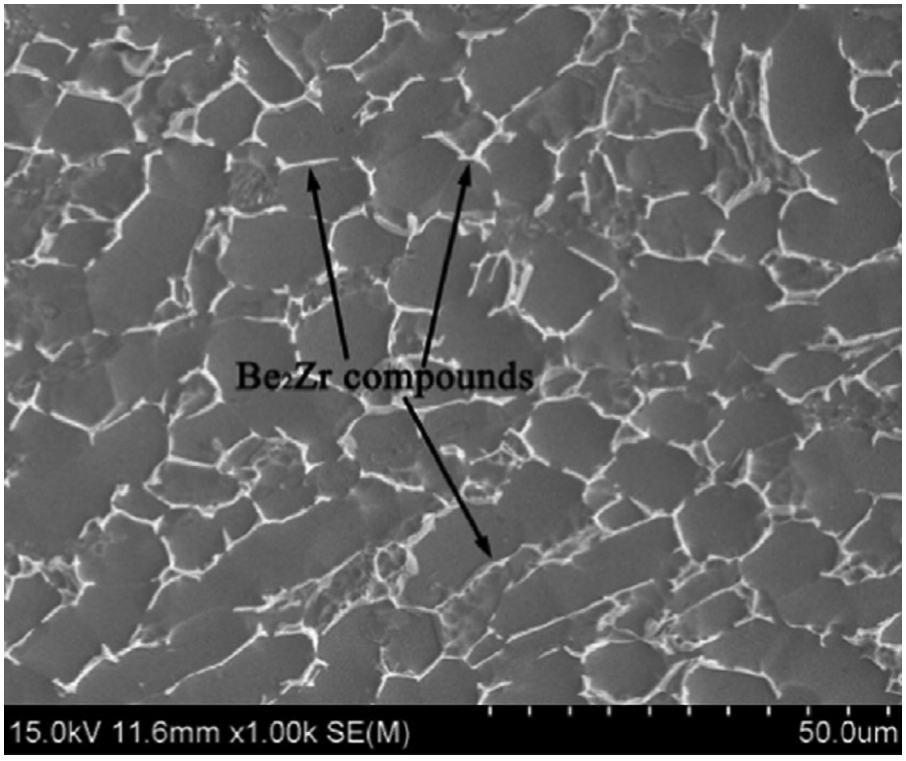

Fig. 9. Scanning electron microscopy (SEM) micrograph of. Zr-5Be (at.%) alloy hot rolled and annealed at 850 °C for 2 h taken from Ref. [114].

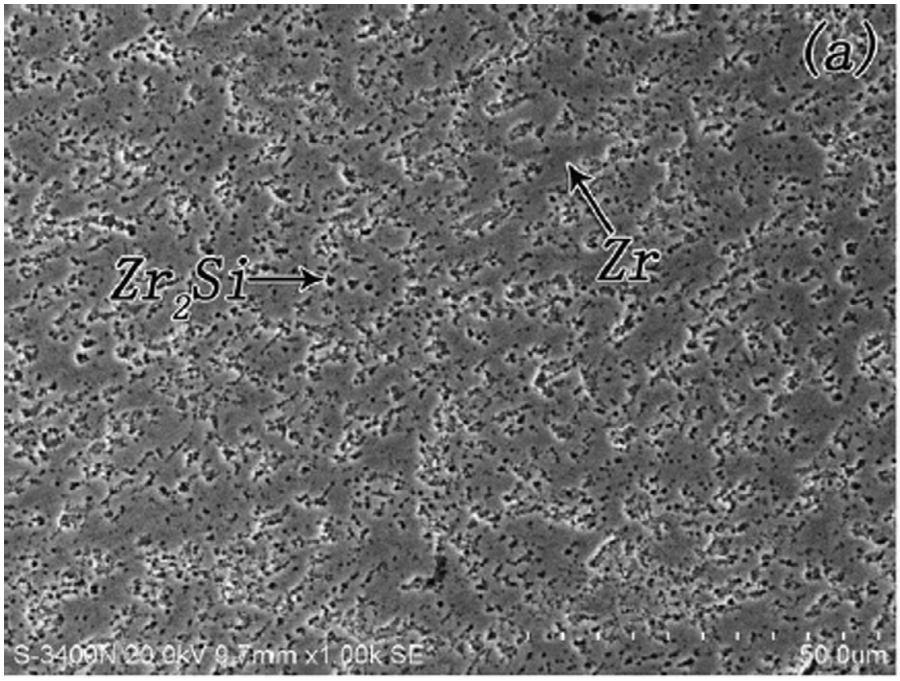

Fig. 10. Secondary electron SEM micrograph of as cast Zr–8.8Si. Taken from Ref. [120].

Dissolution of secondary phase particles is known to occur at high fluence ($>10^{26}$ n·m^{-2}, 20 dpa) due to the effects of displacive radiation. A correlation between an increase in Fe content and <*c*>-loop dislocation size and density has been made, suggesting that Fe will promote irradiation induced growth [172]. It is unclear as to whether this will translate to fusion environments as thermal creep will likely dominate. However, success in increasing Fe content in conventional Zr alloys (to ~0.50 wt.%) has been seen in HiFi^{TM} for lowering H pickup in fission environments [173].

3.1.9. Zr-Mo

Molybdenum has a large high-temperature solubility in β-Zr ($\leq$20 at.% at 1576 °C) but is not soluble below 730 °C in α-Zr. Experimental studies on binary alloys of the two species are typically made on quenched samples from the β-phase forming region and are considered for room temperature biomedical applications [122]. At intermediate temperatures (500–730 °C) the C15 $ZrMo_2$ Laves phase will form [174]. The mechanical properties of two binary mixtures with 0.2 and 1.0 at.% Mo, which were cold worked,

annealed at 750 °C for 1 h then annealed at 500–550 °C for 3 h, have been measured at 400 °C. It was observed that a linear increase in yield strength from 60 to 130 MPa could be achieved with increasing Mo content compared to ~20 MPa of the base metal [123]. Hydrogenation experiments on these samples were also conducted and it was shown that the H retention decreased with increasing Mo content and when Mo is included at ~1.0 at.% the corrosion resistance of the material, in water at 350 °C, is significantly improved compared to 0.2 and 0.5 at.% mixtures. It is thought that the $ZrMo_2$ has a low H absorbency, which is the main contributing factor to the decrease in H retention. In these samples, it is possible that there is a β phase fraction still present as ageing studies of Zr alloys containing Mo have shown that complete transformation from $\beta \rightarrow \alpha$ phase occurs by 1000 h yet some β phase is still retained after 100 h [175].

3.1.10. Zr-V

Vanadium has a small solubility in α-Zr (1–3 at.% below 863 °C) [176]. Above this concentration the V_2Zr C15 Laves phase forms [176], and above 863 °C a single phase BCC solid solution will form, which has a solubility of $\leq$18 at.%.

The mechanical properties of alloys containing 0.2 and 0.5 at.% have been studied previously [124]. The samples were hot-rolled at 870 °C and quenched, and as a result of the quenching, some β phase was retained. Both samples displayed an $\alpha+\beta$ microstructure and exhibited strengths of 700 MPa and 820 MPa and elongation of 17% and 20%, respectively. It is expected that the β phase will not remain, and V_2Zr precipitation will occur if used in long term operation between 500 and 700 °C.

3.1.11. Zr-W

Tungsten has a limited solubility (1–3 at.% below 850 °C) in α-Zr and will form the W_2Zr C15 Laves phase outside these compositional bounds. Above 850 °C, W is soluble in β-Zr up to ~5 at.% [177].

A study reporting the mechanical properties of powder processed (34–57 at.% W) samples reported large compressive strengths at room temperature (1060–2690 MPa) however these samples were very brittle where fracture at <1.0% tensile strains occurred, attributed to porous defective structures [125].

3.2. Higher order Zr alloys

Higher order advanced Zr based structural alloys with improved room temperature mechanical properties are a topic of interest in the biomedical community due to their lower magnetic susceptibility, relative to Ti, and biocompatibility for implants [178]. However, it is the room temperature mechanical properties of single β phase alloys that are of interest to this community, and the target for a bulk moduli is 10–30 MPa for their application as implants/prosthetics. Therefore, ageing studies at intermediate temperatures (500–700 °C) are not typically performed and instead quenching from ~1000 °C is routine. Furthermore, the compositions are typically highly alloyed and present large thermal neutron absorption cross-sections. Nevertheless, the state-of-art pertaining to each higher order Zr alloy identified for this review is presented in the following subsections. Table 4, provides a summary of available scientific literature and score calculated identically to the binary systems. No mechanical property data for >RT were found within this review.

3.2.1. Zr-Ti-Al-(V)

Several investigations into the mechanical properties of ternary Zr-Ti-Al alloys have been conducted to-date. However, the focus has been on Ti rich compositions where the alloy with the highest concentration of Zr was 45Ti-40Zr-15Al (at.%). The trend of decreasing $\alpha \rightarrow \beta$ transition temperature as the ratio between Ti:Zr approaches one, remains true when Al is included in the concentrations studied ($\leq$15 at.%) [179]. Conversely, Al additions increase the transition temperature [180]; a concept in agreement with the α-Ti stabilising effect of Al addition observed in the past. The microstructures of the Zr-Ti-Al alloys are highly dependant on cooling rate and processing conditions and single phase α, β or multiphase α' (β transformed α) and α'' (metastable orthorhombic) microstructures have been demonstrated for similar compositions [180,181]. Only the room temperature mechanical properties have been assessed, where UTS ranges from 1000 to 1550 MPa with 3–11% uniform elongation.

Exploration of the compositions that include V, in the Zr-Ti-Al-V system, originated with Ti-6Al-4 V wt.% (Ti-6–4), a dual phase $\alpha+\beta$ Ti alloy used for aerospace and biomedical applications [182]. In the initial study, 8–28 at.% Zr was added to the Ti-6–4 alloy composition [183]. The maximum UTS was measured to be 1317 MPa (increase of 320 MPa compared to Ti-6–4) and elongation of 8% (decrease of 6% compared to Ti-6–4), at room temperature. An additional study reporting the microstructures and mechanical properties of a series of alloys with higher Zr contents (Table 5) within the Zr–Ti–Al–V system was published [184]. These samples were annealed at 850 °C for 30 min, hot rolled, and quenched. Non-equilibrium microstructures of α' and α'' (metastable orthorhombic) were observed in combination with the β phase for the samples with lowest and second lowest Zr content, respectively. The three Zr richer samples had mixtures of α and β phase. The room temperature UTS peaked at 1246 MPa for Zr–45Ti–5Al–3 V wt.% and stemmed a new branch of research into this composition and its variations where some are referred to as TZAV. The $\alpha \rightarrow \beta$ transition temperature was investigated in the original study where it was determined that as the Zr content increases, the transition temperature decreases in line with the behaviour of a binary Zr-Ti alloy. Although similar experiments have not been carried out on compositions with >>50 at.% Zr, it is expected that the $\alpha \rightarrow \beta$ transition temperature will increase when the Zr:Ti ratio is >>1. However, precipitation of the Zr_3Al phase is likely due to the reduced solubility of Al in Zr compared to Ti.

An investigation into the microstructure after ageing at 500, 550, and 600 °C for 32 h has been made on the Zr–45Ti–5Al–3 V (wt.%) alloy after solution treatment at 850 and 1050 °C [185]. It was determined that regardless of prior solution treatment, the fraction of α-phase changed dramatically within the first 32 h, see Fig. 11. As pictured, the β-phase was partially retained in the 550, and 600 °C aged samples but 100% of α-phase was recovered after ageing at 500 °C. Phase changes of this scale, at temperatures relevant to breeder operation, would be undesirable in a structural material.

An additional study on the Zr–45Ti–5Al–3 V (wt.%) alloy has been made comparing the microstructure and room temperature mechanical properties after annealing samples for 1 h at 500, 600, 700, and 800 °C, after homogenisation and quench from 1000 °C. The annealed samples were cooled in air (at a rate of 10 $°C \cdot s^{-1}$) and in a furnace (0.07 $°C \cdot s^{-1}$) [186]. It was found that the samples that were air cooled to RT from temperatures between 500 and 800 °C had drastically reduced total elongations (1–3% from 5.4% in the as-forged state) whereas the samples that were furnace cooled increased in ductility, displaying higher total elongations at RT (6–10%), see Fig. 12. This was attributed to the athermal $\underline{\omega}$-phase formation during the more rapid cooling. These results are also supported by a separate study with a similar conclusion on the Zr-40Ti-5Al-4 V (wt.%) composition [187]. From these results it may be possible to hypothesise that if such cooling rates occur in a breeder blanket during pulsed operation the structural material may embrittle significantly.

Variations of this system have been made with the addition of Fe in concentrations 0.5–2.5 wt.% [188] and replacement of V

Table 4
Checklist and tally of the type of data identified within this review to be available within the scientific literature for each higher order Zr system. RT, σ and ε refer to room temperature, stress, and strain, respectively.

Alloy	Microstructure			Mechanical properties	Score	*Pros*	*Cons*	Future work
	As-cast	Heat treated 500–700 °C	Heat treated >700 °C	RT σ vs ε				
Zr-Ti-Al-(V)	√ [112–114]	√ [115–117]	√ [115–119]	√ [112,113,115,116,118,119]	4	• Good room temperature strength and ductility when furnace cooled. • Can be tailored for $\alpha+\beta$ microstructure at 550–600 °C that may provide creep resistance. • The activity of alloying elements within this system are lower than that of pure Zr, ranging from 10^7 to 10^9 Bq·kg^{-1}	• High Ti content will equate to high thermal neutron absorption cross-sections (compositions studied ~2.5 bn). • Faster cooling rates will induce brittle ω phase formation. • β-phase can completely transform to α-phase if ageing occurs past 32 h at 500 °C.	• Reduce Ti and V content, to minor alloying additions, to reduce thermal neutron absorption cross-section. • Mechanical property tests should be conducted at elevated temperatures.
Zr-Al-Sn	√ [120]		√ [120]	√ [120]	3	• Low thermal neutron absorption cross-section. • Good as-cast and heat treated mechanical properties at room temperature.	• Potential susceptibility to corrosion in aqueous environments. • Alloying additions of Sn will increase the activity of the alloy.	• Ageing experiments between 500 and 700 °C should be performed to identify Zr-Al precipitate structures and stabilities. • Mechanical properties should be evaluated at RT and elevated temperatures.
Zr-Mo-Ti	√ [121]			√ [121]	2	• Has the potential to precipitate harden and solid solution strengthen. • May be more resistant to H absorption. • Good β-phase room temperature mechanical properties.	• High thermal neutron absorption cross-section (compositions studied ~1.0 bn). • No microstructural or mechanical property literature exists for temperatures between 500 and 700 °C. • Mo additions will significantly increase the activity.	• Reduction of alloying species and microstructural/mechanical property investigations at temperatures between 500 and 700 °C.
Zr-Nb-Ti	√ [122,123]			√ [122,123]	2	• Good room temperature mechanical properties of the β-phase.	• High thermal neutron absorption cross-section. • Higher alloying (therefore higher neutron cross-section) is required to stabilise β-(Nb,Zr,Ti) phase below 600 °C. • Additions of Nb will increase activity of alloy.	• Reduce alloying. • Addition of species to alloy with the BCC Nb phase.
Zr-Mo-(Sn)			√ [108]	√ [108]	2	• Relatively good thermal neutron absorption cross-section. • Good room temperature strength with microstructures equilibrated at 500 °C.	• Brittle at room temperature. • Mo will significantly increase activity of the alloy.	• Detailed crystallographic and microstructural analyses to determine cause of embrittlement. • Investigate role of cooling rate on microstructure.

Table 5
Example compositions (at.%) of alloys investigated in the Zr-Ti-Al-V system [184].

Zr	Ti	Al	V	UTS (MPa)	Elongation (%)	$\alpha \rightarrow \beta$ transition temperature (°C)
17.3	69.2	~10.0	~3.5	1168	3	~800
26.0	60.5			1206	10	~675
34.5	52.0			1246	12	~625
43.3	43.2			1040	13	~575
51.9	34.6			978	11	~500

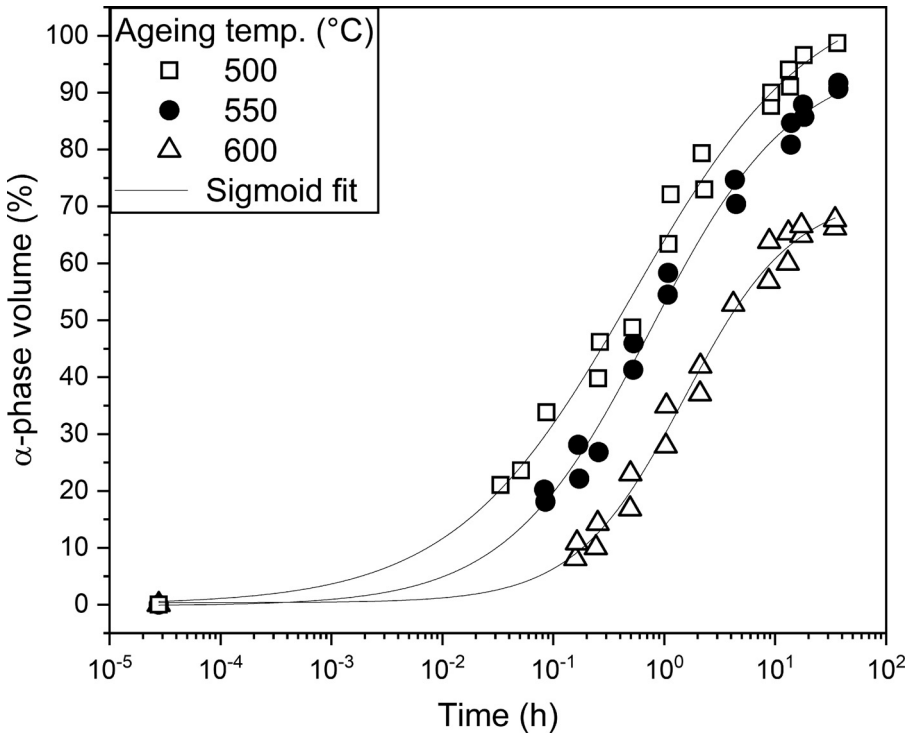

Fig. 11. Volume fraction of α-phase measured by XRD for Zr–45Ti–5Al–3 V (wt.%) when aged at 500 °C (squares), 550 °C (circles), and 600 °C (triangles). Curves fitted using sigmoid functions [185].

with Fe in concentrations of 0.5–2.0 wt.% [189]. However, ageing experiments have not been conducted at 500–700 °C and only non-equilibrium microstructures, with high β phase fractions, quenched from a high temperature ≥850 °C have been assessed. It is likely that at temperatures relevant to a breeder blanket the Zr_3Fe or TiFe intermetallic will precipitate due to the insolubility of Fe in α-(Zr,Ti). Further work is required to determine the material behaviour at the relevant temperature range.

The thermal creep properties of the Zr-Ti-Al-V system have not been assessed, however, due to the similarities of Zr and Ti, and substantial amounts of literature on the creep of Ti-6–4 we may draw some insights into the possible behaviour.

The creep process in Ti-6–4 is suggested to be dominated by climb processes of α-phase dislocations in the prismatic plane ($<a>$ loops) [190,191]. It should be noted that in Ti alloys, the β-phase generally exhibits faster diffusion than α and so the volume fraction of β is often minimised in high temperature Ti alloys [192]. Nevertheless, dual-phase $\alpha + \beta$ microstructures are effective in both Ti and Zr materials for conferring high strength ~1000 MPa and good creep resistance ~400 °C. However, for every 100 °C increase, the creep rate increases by over an order of magnitude, and at ~525 °C the steady-state creep strain rate is $>10^{-6}$ s^{-1} for applied stresses ≥70 MPa [191], see Fig. 13. Moreover, the thermal creep rates above 500 °C are likely too high for use of these materials in a breeder blanket.

3.2.2. Zr-Al-Sn

One study has been conducted on alloys within the Zr-5Al-(2–6)Sn (wt.%) composition range in the context of structural nuclear materials [193]. A single α phase, lath martensitic structure was identified with compressive yield strengths and strains ranging from 835 to 913 MPa and 18.57–21.43%, respectively. Heat treating for 2 h at 900 °C and air cooling led to the precipitation of ZrAl (orthorhombic), which is likely metastable as one would expect Zr_3Al from binary phase diagrams. Nevertheless, the RT compressive yield strengths were increased to 1003–1044 MPa and the strains decreased to 13.03–18.79%.

3.2.3. Zr-Mo-Ti

Alloys within the Zr-Mo-Ti ternary have been investigated by the biomedical research community [194]. The compositions Zr-12Mo-(3–11)Ti were quenched from the melt and only single phase β microstructures were observed. The room temperature yield strengths were found to range from 1200 to 1363 MPa, and the strains to failure ranged from 12 to 20%, when in compression. However, it is not expected that these compositions would retain their single phase β microstructures at operation temperatures in a breeder blanket. Instead multiphase microstructure of α-(Zr,Ti), $ZrMo_2$ and/or β-(Zr,Ti,Mo) is predicted to occur. It is likely that this, along with possible ω phase at non-quench cooling rates, will

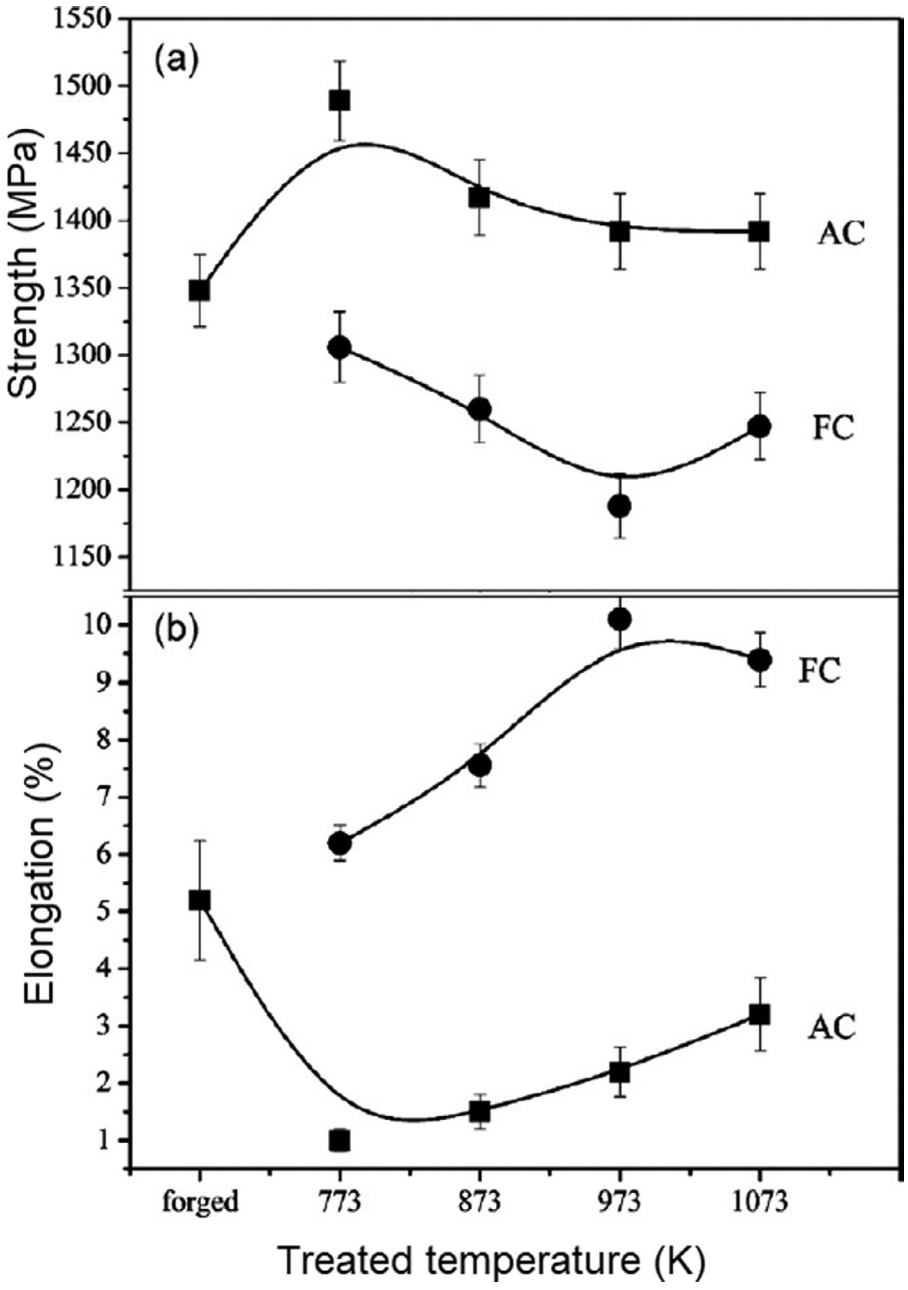

Fig. 12. Strength and elongation of Zr–45Ti–5Al–3 V (wt.%) after annealing at different temperatures (x-axis) for 1 h and air cooling (squares) or furnace cooling (circles) to RT. Taken from Ref. [186].

contribute greatly to strengthening and the ductility will be reduced further.

3.2.4. Zr-Nb-Ti

The compositions that have been investigated to-date are Zr-20Nb-(3–15)Ti [195] and Zr–12Nb–(2–16)Ti [196]. All samples were observed to consist of a single-phase BCC structure except Zr-12Nb-16Ti, which exhibited some ω-phase. Relatively good mechanical properties were achieved with strengths ranging from 1000 to 1300 MPa and compressive strains of ~35%.

A majority of the lower Ti compositions exist outside the single-phase forming region and will undergo transformations from $\beta \rightarrow \alpha/\alpha'$ if operated at temperatures ~550 °C [159]. However, for higher Nb and Ti contents it may be possible for the single phase β forming region for this ternary system to exist at this temperature.

3.2.5. Zr-Mo-(Sn)

Alloys within the Zr-Mo-Sn ternary system were investigated in the 1950–70 s in the context of high temperature (500 °C) structural materials for fission applications [175]. It was the aim of the investigators to quench the Zr-2.8Mo-1.5Sn (at.%) composition from the $\alpha + \beta$ (850 °C) and β (1000 °C) forming regions, anneal at 500 °C for 1000 h, and retain a strong high temperature β or transformed (α') phase while maintaining room temperature ductility. The composition tested was Zr-2.8Mo-1.5Sn (at.%). It was reported that for the sample quenched from the β forming region, an $\alpha + \alpha'$ microstructure was produced, and for the sample quenched from the $\alpha + \beta$ forming region, an $\alpha + \alpha' + 10\%\ \beta$ microstructure was produced. However, the UTS/elongation for each sample were measured to be 853 MPa/2.6% and 1023 MPa/2.3%, respectively, which is too brittle for workability of a structural material. There is insufficient data on the crystallographic analyses of these

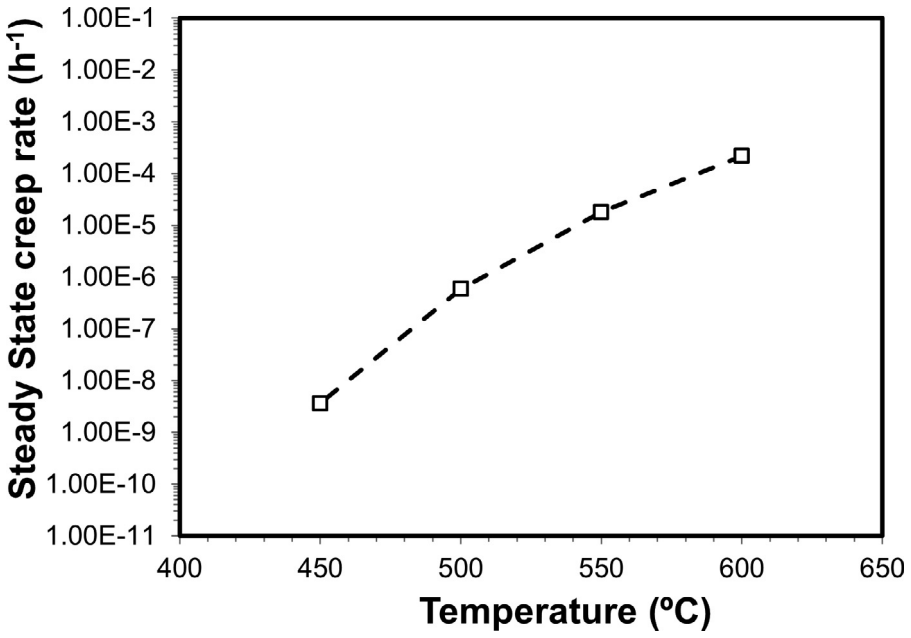

Fig. 13. Estimated steady-state creep rate for an applied stress of 70 MPa for Ti-6–4 extrapolated from data taken from Ref. [191].

samples to discount ω or intermetallic precipitation, which may have led to the reduction in ductility. Alloys containing Nb and V in 2 at.% contributions were also studied and were found to exhibit lower strengths and lower ductility. It should also be mentioned that Zr-4.7Mo-1.5Sn and Zr-1.8Mo-3.0Sn were investigated, however, were only aged for 8–24 h at 482 - 538 °C and therefore likely did not have microstructures or mechanical properties accurately reflecting components in operation at these temperatures.

3.3. Comparison of properties

Fig. 14 shows the room temperature yield strengths and strains to failure of binary and higher order Zr alloys, experimentally measured in the reviewed studies. There are many systems that present a good combination of room temperature strength and ductility. However, this information is not adequate to provide confidence in their ability to maintain structural integrity at higher temperature operation. Some Zr-Al, Zr-V, Zr-Mo-(Ti) and Zr-Nb-Ti compositions can demonstrate comparable uniform elongations and markedly higher RT strengths than Zr-4. However, the latter three alloy systems present significant BCC phase fractions that are likely unstable at operating temperatures between 500 and 700 °C, and the Zr-Al compositions that can achieve ductile behaviour at RT require a polished surface state.

One of the challenges of alloying Zr for nuclear applications is that including most elements in large quantities (>1 at.%) significantly alters the thermal neutron absorption cross-section (σ_{abs}) for which Zr was selected in the first place. A weighted average of the elemental σ_{abs} for each Zr alloy was calculated and plotted against RT yield strength, see Fig. 15. It can be seen that binary Zr alloys containing Al, Be, Sn, Ti and Nb present σ_{abs} values comparable to Zr-4 of 0.2 bn. Zr-Cr, -Mo-Ti, -Nb-Ti, -Ti-Al-V display σ_{abs} values closer to 1.0 bn, which is of similar magnitude to the ^{6}Li breeding cross-section but less than half that of Fe (2.56 bn). Using this method of calculation, the maximum concentration of each element allowed before a binary Zr-X alloy exceeds the σ_{abs} of Zircaloy-4 can be estimated, see Table 6. Only Al, Nb and Sn can be alloyed in concentrations > 1 at.%. Be, Mg and Si have σ_{abs} values lower than Zr therefore have no concentration limit.

When compared to multi-decadal research efforts that have been undertaken for reduced-activation ferritic/martensitic (RAFM) steels, advanced Zr alloy research is in its infancy. Targeted, small-scale, laboratory experiments that investigate microstructure and mechanical properties are still required to make a better judgement as to whether advanced Zr alloys are worth pursuing for use in operating temperatures between 500 and 700 °C. Castable nanostructured steels currently represent the state-of-the-art in RAFM steel research and should be used as a mechanical property benchmark for any future Zr alloys investigated for a similar purpose. A comprehensive overview of the history and current status of RAFM steels can be found in Ref. [197].

3.4. High-entropy alloys

High-Entropy Alloys (HEAs), or complex concentrated alloys (CCAs) are alloys consisting of ≥4 elements in near equiatomic concentrations [198]. This relatively new area of study has seen tremendous growth over the last 10 years. The original premise of HEAs is that a solid solution phase is stabilised by the configurational entropy (entropy of mixing), which increases in magnitude with the addition of more elements, and is maximised when their concentrations are in equal ratio [199,200]. It is the solid solution phase that is typically the majority phase within a HEA, existing as simple BCC, FCC or HCP structures. The highly alloyed nature of these phases is thought to contribute greatly to solid solution strengthening and allow for higher strengths than conventional alloys while maintaining ductility [201].

Difficulties arise in maintaining the solid solution phase when ageing at temperatures between 400 and 1000 °C. This is because the entropy term is a prefactor to temperature in the equation for Gibbs free energy, and typically stabilises the solid solution phase at temperatures close to melting. Therefore, for lower temperatures more commensurate with that of breeder blanket operation in a fusion reactor, decomposition of the solid solution phase and precipitation of intermetallics is more likely, and is observed to occur in many ageing/annealing experiments for HEAs [202–205]. Whilst assessments of the room temperature properties of as-cast/solution treated and quenched HEAs is commonly performed, a significantly smaller fraction of thermal ageing studies have been performed

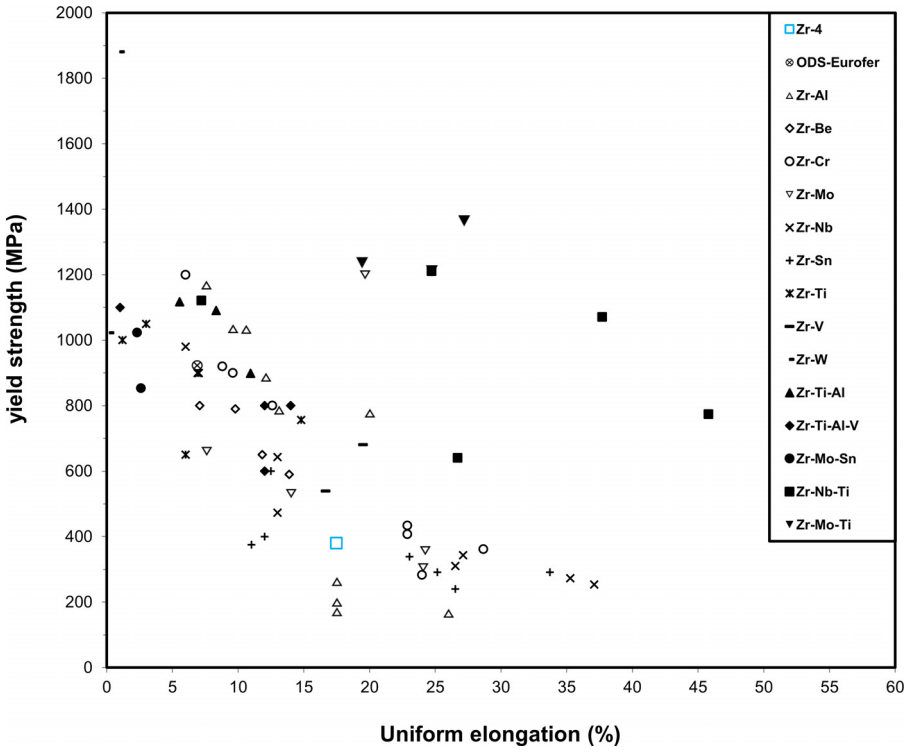

Fig. 14. Room temperature yield strengths of pure Zr, commercial, binary, and higher order Zr alloys and their tensile strains to failure. The dataset used to construct this figure is accessible from Ref. [8].

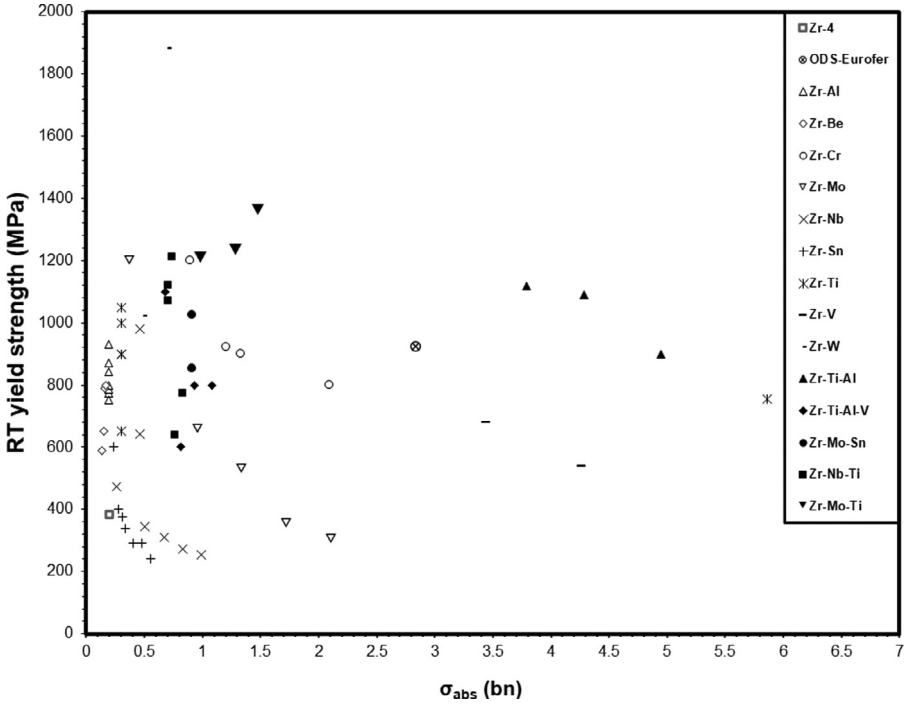

Fig. 15. Room temperature yield strength of experimentally measured alloys plotted against their theoretical thermal neutron absorption cross-sections.

Table 6
Maximum allowable concentration of element before thermal neutron absorption cross-section exceeds that of Zr-4 (0.3 bn) in a binary alloy.

	Al	Be	Cr	Fe	Hf	Mg	Mo	Nb	Ni	Os	Pd
at.%	32.61	–	0.52	0.63	0.01	–	0.65	1.55	0.35	0.09	0.22
	Re	Ru	Sc	Si	Sn	Ta	Ti	V	W	Y	
at.%	0.02	0.63	0.05	–	3.40	0.07	0.25	0.31	0.08	1.37	

on HEAs, and fewer still assess mechanical properties of equilibrium microstructures at elevated temperatures [206]. Nevertheless, very high strengths (~2.3 GPa) have been observed in BCC HEAs that also show a higher resistance to softening than Ni superalloys at elevated temperatures (500–1000 °C) [206,207]. Further, some HEAs are reported to have good tolerance to irradiation damage [208,209].

In the context of Zr alloys for fusion, by definition a HEA cannot contain a majority portion of Zr in the mixture and therefore the σ_{abs} will largely depend on the other elements in the alloy. The Nb-Ti-V-Zr system has been identified as one of the single phase HEA systems with the lowest σ_{abs}, which is still on the order of steels [210]. It may be possible that the increased strength of such alloys is sufficiently high that a reduced amount of structural fraction can be used and therefore less absorption of neutrons compared to other candidate materials. However, if a very low σ_{abs} ($\leq$0.2 bn) HEA is desired it would be based upon the low $\sigma_{abs,}$ elements Al, Be, Mg, Pb, and Si, with Zr, where a single-phase solid solution is unlikely to be achievable due to the largely favourable formation energies for intermetallic compounds. The binary mixtures alone present many different possible intermetallic phases, which amongst them are some ordered HCP structures, e.g., Zr_3Al, Be_2Zr, Zr_5Pb_3, that may maintain some measure of ductility. However, the low melting temperatures of Al, Mg, and Pb are a concern. Nevertheless, opportunities still may exist in multi-phase low σ_{abs} HEAs.

Pros: BCC refractory metal HEAs can exhibit high strengths and resistance to softening at higher temperatures, and further, some HEAs may be resistant to irradiation damage.

Cons: Zr will not contribute a majority concentration to the alloy and therefore the thermal neutron absorption cross-section will rely on the other alloying species, this leads to previously studied HEAs, which have cross-sections comparable to steel. Therefore, the alloying species are restricted to Al, Be, Mg, Pb, and Si if a maintenance of $\leq$0.2 bn is desired, however, these are likely to be low melting temperatures multiphase, and brittle.

Future work: Investigations into multiphase, low σ_{abs} (0.2 bn) HEAs formed between Zr, Al, Be, Mg, Pb, and Si species or very high strength, moderate σ_{abs} (2.0 bn) HEAs should be made and their microstructures and mechanical properties assessed from RT to 700 °C.

4. Summary and conclusions

Zirconium alloys have seen prevalent use in the nuclear industry for power generation by fission. This is largely due to its low thermal neutron absorption cross-section (σ_{abs}). Past publications have alluded to the utility of Zr alloys in a fusion reactor [1,24]. Indeed, the utilisation of Zr alloys would be of great benefit due to their current production in tonnage quantities with a very well established industry that works to nuclear standards with associated well developed machining, inspection techniques, and knowledge base. Thus enabling rapid screening of current commercial Zr alloys for fusion.

Here, we predict that by using Zr-4 as a structural material in the breeder blanket, the tritium breeding ratio (TBR) is markedly improved over other candidate materials (EUROFER 97, V-4Cr-4Ti, SiC/SiC) for structural fractions $\leq$0.8. However, current commercial Zr alloys do not have adequate strength, creep resistance, and fatigue properties at the temperatures of 500–700 °C, at which some blanket designs in DEMO-like fusion reactors are expected to operate [5,9]. Further, embrittlement due to impurity elements such as H, He and corrosion from the coolant will likely occur and barrier coatings between the structural alloy/plasma, /breeder and /coolant will need to be employed. For these reasons, the use of Zr alloys may be more suited to a water-cooled lithium lead (WCLL) breeder blanket concept, which operates in the temperature range 280–325 °C and nominal for fission reactors. However, this review was conducted to explore the landscape and potential of novel Zr alloys that can achieve adequate mechanical properties at temperatures beyond current fission reactors, between 500 and 700 °C.

Initial screening of the mechanical properties and thermal neutron absorption cross-sections of advanced Zr alloys has identified systems that have demonstrated adequate room temperature properties. Of these systems, Zr-Al has been studied the most extensively for its potential use as a Zr_3Al structural intermetallic cladding material in fission applications. Some compositions have been reported to achieve room temperature ductility ($\geq$5% uniform elongation), high strength ($\geq$800 MPa), resistance to high temperature softening, and good creep resistance. However, ductility issues arise in unpolished components, and poor corrosion resistance is noted in aqueous environments. Any additional development of these alloys should be done through alloying of other species, in an attempt to address these shortcomings.

Historically, the alloying of Sn and Zr is an attractive method of increasing creep resistance in conventional Zr alloys while maintaining a low thermal neutron cross-section. However, in the binary form it offers inadequate strengthening. There is potential for future work in the Zr-Al-Sn system as it has a very low thermal neutron absorption cross-section and is strengthened by solid solution and precipitation while maintaining a ductile nature at room temperature. However, such a system is likely to be susceptible to aqueous corrosion and is better suited to breeder blankets with non-aqueous cooling systems. Alternatively, the mixture of Nb and/or O in Zr alloys may provide an option for resistance to aqueous corrosion and H pickup.

A common theme amongst the studies to-date is that microstructural and mechanical property data pertaining to samples aged at temperatures relevant to a breeder blanket (500–700 °C) is lacking. Instead, the majority of studies quench from the annealed condition in the β-phase forming region (800–1000 °C). Long term operation at temperatures below the β-phase solvus will decompose the β-phase and therefore these studies are not a good indicator of material performance at the proposed temperatures.

To preserve the low σ_{abs} that Zr alloys are known for, only Al, Be, Nb, Si, Sn and Y can be alloyed in concentrations >1 at.%. Equilibrium microstructures are important to characterise at temperatures between 500 and 700 °C due to kinetics being sufficient for equilibrium to be achieved. Therefore, precipitate structures, morphologies and their influence on mechanical properties must also be characterised. When an alloy is identified that can maintain adequate strength ($\geq$400 MPa) at this temperature range, tertiary screening, i.e. creep, irradiation testing, corrosion from aqueous and liquid metals (Li/Pb) and H/He embrittlement, should be conducted. It is recommended that higher order Zr alloys combining the aforementioned low σ_{abs} elements are explored, especially as Be has been shown to strengthen but not embrittle and increase corrosion resistance, and Si has potential to do the same.

In terms of nuclear waste production, Zr alloys are predicted to decay cool to an activity of $\sim 10^8$ ($Bq \cdot kg^{-1}$) after 100 years post-service, nearly an order of magnitude larger than EUROFER 97, where both fail to meet the UK fusion low level waste limit. We suggest that it may not be practicable to produce a Zr based component that both meets the proposed mechanical and waste requirements for a breeder blanket. Further, some of the recommended low thermal absorption neutron cross-section elements (Be, Nb, and Sn) will increase the activity of such components. Therefore, an approach of "as low as reasonably practicable" may be more suitable in order to harness the neutron efficiency advantage of Zr for tritium breeding. Further cost-benefit analysis is required in this area.

Declaration of Competing Interest

The authors declare that they have no known competing financial interests or personal relationships that could have appeared to influence the work reported in this paper.

CRediT authorship contribution statement

D.J.M. King: Writing – original draft, Writing – review & editing, Formal analysis, Investigation, Data curation, Visualization, Project administration. **A.J. Knowles:** Conceptualization, Writing – original draft, Writing – review & editing. **D. Bowden:** Conceptualization, Writing – review & editing. **M.R. Wenman:** Supervision, Writing – review & editing. **S. Capp:** Data curation. **M. Gorley:** Writing – review & editing. **J. Shimwell:** Methodology, Formal analysis, Writing – review & editing, Visualization, Resources, Software. **L. Packer:** Writing – review & editing. **M.R. Gilbert:** Methodology, Formal analysis, Writing – review & editing, Visualization, Resources, Software. **A. Harte:** Conceptualization, Resources, Writing – review & editing, Supervision, Project administration, Funding acquisition.

Acknowledgements

The Authors would like to acknowledge funding from EPSRC (EP/T012250/1) and (EP/S01702X/1) for time and resources. As well as Profs. Ted Derby, Michael Preuss, Erland Schulson, and Steven Zinkle for discussion regarding subject matter of this review.

A Knowles acknowledges funding & support from: UKRI Future Leaders Fellowship (MR/T019174/1), Royal Academy of Engineering Research Fellowship, EUROfusion Researcher Grant, and EPSRC (EP/T01220X/1).

Acknowledgement to authors of internal reports, used to guide the writing of this review, should also be given. These people include: F. Barton, J Bernard, F. Lowrie, C. Riley and M. Rogers from Rolls-Royce plc, and P. Binks, S. Foster and M. Green from the John Wood Group plc.

Appendix

A simple spherical blanket model was created in OpenMC [1] using Constructive Solid Geometry (CSG) to ascertain the relative impact of different blanket material configurations on the tritium breeding ratio (TBR). The simplified model resembles inertial confinement fusion (ICF) reactors but avoids the introduction of design specific choices such as lack of inboard blankets and limits its bias in the study. The aim is to provide relative TBR values as a stage in the process of down selecting from a wide range of materials, material fractions and dimensions. The radius of the vacuum region between neutron source and first wall is 10 m, the first wall armour and first wall thickness was based on Ref. [2] and set to 3 mm and 2.7 cm, respectively, and the blanket thickness was set at 2 m. A point source with a Muir energy distribution around 14.06 MeV was used to approximate a deuterium-tritium plasma neutron source, which is an available source term in OpenMC [4]. No backing was applied to the breeder zone to avoid biasing the result towards a design that depends on a reflection of neutrons. Nuclear data was used in from the following sources in the following order of preference Fendl 3.1d [6], Je_ 3.3 [7] and ENDF 7.1 [8].

The neutronics material maker [5] was used to create individual materials as it takes account of variables such as temperature, pressure and ^{6}Li enrichment when calculating material densities. The impacts the density of lithium lead and helium coolant is important to account for this when performing parameter scans. The amount of individual simulations required to accurately cover the parameter space is significant. To mitigate this, an adaptive sampling technique [9] was used to accurately cover the parameter range with a minimal number of simulations.

The material composition and volume fractions of the firstwall were fixed according to Table A1. The volume fractions of the structural and breeding material in the breeding zone were varied from 0 to 0.9. However, the volume fraction of the coolant in the breeder zone was fixed at 0.1, see Table A2. The breeder material was chosen as liquid Li-Pb ($Pb_{84.2}Li_{15.8}$), due to the fact that ce-

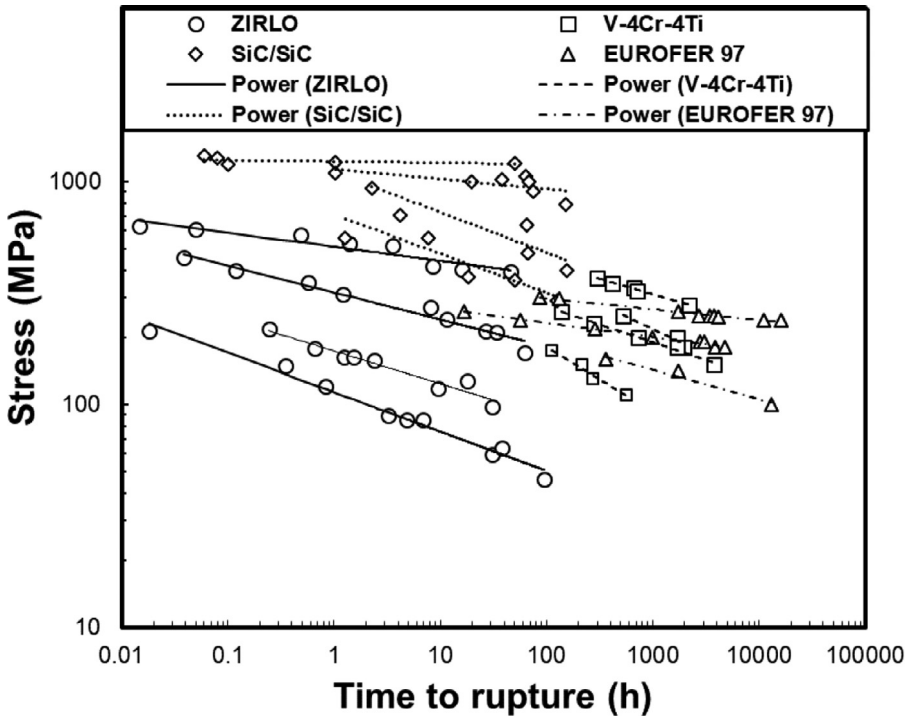

Fig. A1. Time to rupture of ZIRLO^{TM} (circle), V-4Cr-4Ti (square), SiC/SiC (diamond) and EUROFER 97 (triangle) with.

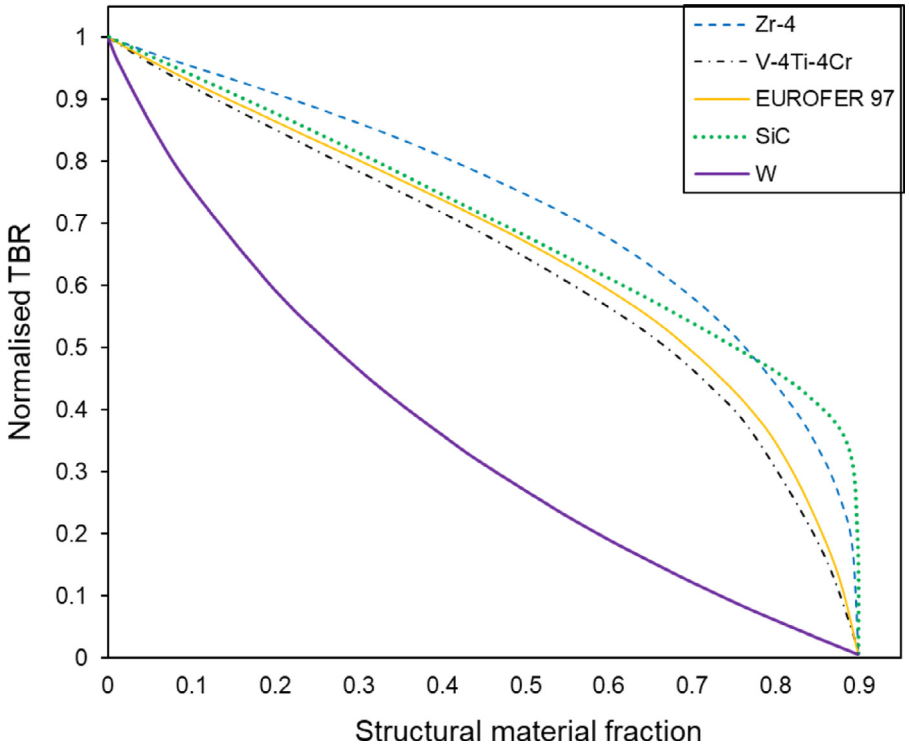

Fig. A2. The relative TBR with 0.9 ^{6}Li enrichment fraction for the WCLL design for different structural materials in the breeder blanket and the structural material fraction varied.

Table A1
First wall composition, densities calculated using neutronics material maker [5].

Material	density (g/cm^3)	volume fraction
Tungsten	19	0.106305
EUROFER 97	7.78	0.560188
Water at 15.5 × 10^6 Pa and 305 °C	0.72	0.333507
Helium at 8 × 10^6 Pa and 500 °C	0.0056	0.333507

Table A2
Breeder zone composition, densities calculated using neutronics material maker [5].

Material	density (g/cm^3)	volume fraction
Variable structural material	variable	variable
Lithium-lead at 500 °C	9.15	variable

Table A3
Structural materials used in the simulation.

Structural material	density (g/cm^3)	elements and weight percents
EUROFER 97	7.8	Fe 89.27, C 0.11, Mn 0.4, Cr 9, Ta 0.12, W 1.1
Iron	7.87	Fe 100
SiC	2.7	Si 50, C 50
Vanadium	5.8	V 100
Vanadium 4	6.05	V 92, Cr 4, Ti, 4
Tungsten	19.3	W 100
Zircaloy 4	6.56	Zr 98.2, Sn 1.5, Fe 0.2, Cr 0.1
Zirconium	6.51	Zr 100
Zr_3Al	5.91	Zr 75, Al 25

ramic breeders impose additional dimensions such as packing fraction and multiplier fraction. The ^{6}Li enrichment was also been varied (from 0 to 100%) for this study. The specific structural materials that were investigated can be found in Table A3. The structural materials were homogenised together with a coolant and a breeder material to resemble a helium cooled lithium lead (HCLL) blanket design but is not a substitute for parameter studies performed on a specific heterogeneous design such as in Ref. [3].

References

[1] T.R. Barrett, G. Ellwood, G. Pérez, M. Kovari, M. Fursdon, F. Domptail, S. Kirk, S.C. McIntosh, S. Roberts, S. Zheng, Progress in the engineering design and assessment of the European DEMO first wall and divertor plasma facing components, Fusion Eng. Des. 109 (2016) 917–924.
[2] M. Sandzelius, Fusion Potential For Spherical and Compact Tokamaks (Master's thesis), Royal Institute of Technology, Stockholm, 2003.
[3] A. Sykes, A.E. Costley, C.G. Windsor, O. Asunta, G. Brittles, P. Buxton, V. Chuyanov, J.W. Connor, M.P. Gryaznevich, B. Huang, Compact fusion energy based on the spherical tokamak, Nucl. Fusion 58 (2017) 16039.
[4] P.H. Rebut, ITER: the first experimental fusion reactor, Fusion Eng. Des. 30 (1995) 85–118.
[5] G. Federici, R. Kemp, D. Ward, C. Bachmann, T. Franke, S. Gonzalez, C. Lowry, M. Gadomska, J. Harman, B. Meszaros, Overview of EU DEMO design and R&D activities, Fusion Eng. Des. 89 (2014) 882–889.
[6] E. Gibney, UK hatches plan to build world's first fusion power plant, Nature (2019), doi:10.1038/d41586-019-03039-9.
[7] Z. Shanliang, W. Yican, Neutronic comparison of tritium-breeding performance of candidate tritium-breeding materials, Plasma Sci. Technol. 5 (2003) 1995.
[8] D.J.M. King, High Temperature Zirconium Alloys for Fusion Energy Dataset, Mendeley Data, V1, 2020.
[9] T. Ihli, T.K. Basu, L.M. Giancarli, S. Konishi, S. Malang, F. Najmabadi, S. Nishio, A.R. Raffray, C.V.S. Rao, A. Sagara, Review of blanket designs for advanced fusion reactors, Fusion Eng. Des. 83 (2008) 912–919.
[10] M. Nakamura, K. Tobita, Y. Someya, H. Tanigawa, W. Gulden, Y. Sakamoto, T. Araki, K. Watanabe, H. Matsumiya, K. Ishii, Key aspects of the safety study of a water-cooled fusion DEMO reactor, Plasma Fusion Res. 9 (2014) 1405139.
[11] M.R. Gilbert, S. Zheng, R. Kemp, L.W. Packer, S.L. Dudarev, J.C. Sublet, Comparative assessment of material performance in demo fusion reactors, Fusion Sci. Technol. 66 (2014) 9–17.
[12] K. Ehrlich, The development of structural materials for fusion reactors, Philos. Trans. R. Soc. London. Ser. A Math. Phys. Eng. Sci. 357 (1999) 595–623.

[13] L.M. Giancarli, M.-Y. Ahn, I. Bonnett, C. Boyer, P. Chaudhuri, W. Davis, G. Dell'Orco, M. Iseli, R. Michling, J.C. Neviere, ITER TBM Program and associated system engineering, Fusion Eng. Des. 136 (2018) 815–821.
[14] L.M. Giancarli, X. Bravo, S. Cho, M. Ferrari, T. Hayashi, B.Y. Kim, A. Leal-Pereira, J.P. Martins, M. Merola, R. Pascal, Overview of recent ITER TBM Program activities, Fusion Eng. Des. 158 (2020) 111674.
[15] I. Ricapito, F. Cismondi, G. Federici, Y. Poitevin, M. Zmitko, European TBM programme: first elements of RoX and technical performance assessment for DEMO breeding blankets, Fusion Eng. Des. 156 (2020) 111584.
[16] S. Kass, The development of the zircaloys, Corrosion Zirconium Alloy., ASTM International, 1964.
[17] D.O. Northwood, Irradiation damage in zirconium and its alloys, At. Energy Rev. 15 (1977) 547–610.
[18] D.O. Northwood, R.W. Gilbert, L.E. Bahen, P.M. Kelly, R.G. Blake, A. Jostsons, P.K. Madden, D. Faulkner, W. Bell, R.B. Adamson, Characterization of neutron irradiation damage in zirconium alloys—an international "round-robin" experiment, J. Nucl. Mater. 79 (1979) 379–394.
[19] A. Rogerson, Irradiation growth in zirconium and its alloys, J. Nucl. Mater. 159 (1988) 43–61.
[20] R.B. Adamson, C.E. Coleman, M. Griffiths, Irradiation creep and growth of zirconium alloys: a critical review, J. Nucl. Mater. 521 (2019) 167–244.
[21] D. Kaddour, S. Frechinet, A.F. Gourgues, J.C. Brachet, L. Portier, A. Pineau, Experimental determination of creep properties of zirconium alloys together with phase transformation, Scr. Mater. 51 (2004) 515–519.
[22] C.B.A. Forty, P.J. Karditsas, The potential use of zirconium-based alloys in fusion power plants, in: Proceedings of the 17th IEEE/NPSS Symposium Fusion Engineering (Cat. No.97CH36131), IEEE, 1997, pp. 849–852.
[23] A. Billerey, Evolution of fuel rod support under irradiation–impact on the mechanical behaviour of fuel assemblies, Struct. Behav. Fuel Assem. Water Cool. React. IAEA-TECDOC-1454 (2005) 101–111.
[24] C.B.A. Forty, P.J. Karditsas, Uses of zirconium alloys in fusion applications, J. Nucl. Mater. 283 (2000) 607–610.
[25] Y. Xiao, A.V. Sandwijk, Y. Yang, V. Laging, New routes for the production of reactor grade zirconium, Molten Salts Chem. Technol. (2014) 389–401 1st ed. John Wiley & Sons, Ltd..
[26] K.J. Schulz, J.H. DeYoung, R.R. Seal, D.C. Bradley, Zirconium and Hafnium, in: Critical mineral resources of the United States—Economic and environmental geology and prospects for future supply, Geological Survey, 2018, pp. V3–V26.
[27] H.G. Rickover, L.D. Geiger, B. Lustman, History of the development of zirconium alloys for use in nuclear reactors, Energy Research and Development Administration, Div, Washington, DC (USA), 1975.
[28] ATIAllegheny Technologies Incorporated, Reactor Grade Zirconium, Pittsburgh, 2015.
[29] J.L. Vandegrift, P.M. Price, J.P. Stroud, C.J. Parga, I.J. Van Rooyen, B.J. Jaques, D.P. Butt, Oxidation behavior of zirconium, zircaloy-3, zircaloy-4, Zr-1Nb, and Zr-2.5 Nb in air and oxygen, Nucl. Mater. Energy 20 (2019) 100692.
[30] D.A. Blokhin, V.M. Chernov, A.I. Blokhin, N.A. Demin, I.V. Sipachev, Nuclear physical properties of zirconium alloys E110 and E635 under long-term neutron irradiation in VVER-1000 reactor, Inorg. Mater. Appl. Res. 3 (2012) 124–128.
[31] C.M. Eucken, P.T. Finden, S. Trapp-Pritsching, H.G. Weidinger, Influence of chemical composition on uniform corrosion of zirconium-base alloys in autoclave tests, in: zircon, Nucl. Ind. Eighth Int. Symp. ASTM Int. (1989).
[32] L. Lunde, R.C. Asher, G. Slattery, F.W. Trowse, C. Tyzack, E. Tolksdorf, Zirconium Alloys, U.S. Patent No. 4,212,686, U.S. Patent and Trademark Office, Washington, DC, 1980.
[33] M. Steinbrück, M. Böttcher, Air oxidation of zircaloy-4, M5® and ZIRLO™ cladding alloys at high temperatures, J. Nucl. Mater. 414 (2011) 276–285.
[34] S. Yagnik, A. Garde, Zirconium alloys for LWR fuel cladding and core internals, Struct. Alloy Nucl. Energy Appl. (2019) 247–291.
[35] L.A. Simpson, C.K. Chow, Effect of metallurgical variables and temperature on the fracture toughness of zirconium alloy pressure tubes, Zircon. Nucl. Ind., ASTM Int. (1987) 579–596, doi:10.1520/STP28145S.
[36] P.H. Davies, C.P. Stearns, Fracture toughness testing of Zircaloy-2 pressure tube material with radial hydrides using direct-current potential drop, Fracture Mechanics: Seventeenth Volume, ASTM International, 1986.
[37] A.T. Motta, L. Capolungo, L.Q. Chen, M.N. Cinbiz, M.R. Daymond, D.A. Koss, E. Lacroix, G. Pastore, P.C.A. Simon, M.R. Tonks, Hydrogen in zirconium alloys: a review, J. Nucl. Mater. 518 (2019) 440–460.
[38] V.M. Chernov, B.K. Kardashev, K.A. Moroz, Low-temperature embrittlement and fracture of metals with different crystal lattices–dislocation mechanisms, Nucl. Mater. Energy 9 (2016) 496–501.
[39] R. Liu, W. Zhou, J. Cai, Multiphysics modeling of accident tolerant fuel–cladding U3Si2-FeCrAl performance in a light water reactor, Nucl. Eng. Des. 330 (2018) 106–116.
[40] J. Cheng, Y. Wu, W. Tian, G. Su, S. Qiu, Neutronics and thermo-hydraulic design of supercritical-water cooled solid breeder TBM, Fusion Eng. Des. 92 (2015) 52–58.
[41] IAEA-TECDOC-1496Thermophysical Properties Database of Materials for Light Water Reactors and Heavy Water Reactors, International Atomic Energy Agency, 2006.
[42] B.A. Cheadle, The physical metallurgy of zirconium alloys, At. Energy Can. Ltd. (1975).
[43] R.E. Macherey, C.H. Bean, N.J. Carson Jr, J.R. Lindgren, Manufacture of Fuel Plates For the Experimental Boiling Water Reactor, Argonne National Lab., Lemont, Ill., 1957.
[44] R. Li, P. Zhang, X. Li, C. Zhang, J. Zhao, First-principles study of the behavior of O, N and C impurities in vanadium solids, J. Nucl. Mater. 435 (2013) 71–76.
[45] D.R. Diercks, B.A. Loomis, Alloying and impurity effects in vanadium-base alloys, J. Nucl. Mater. 141 (1986) 1117–1124.
[46] M.L. Grossbeck, J.F. King, D.J. Alexander, P.M. Rice, G.M. Goodwin, Development of techniques for welding V–Cr–Ti alloys, J. Nucl. Mater. 258 (1998) 1369–1374.
[47] R.J. Kurtz, K. Abe, V.M. Chernov, V.A. Kazakov, G.E. Lucas, H. Matsui, T. Muroga, G.R. Odette, D.L. Smith, S.J. Zinkle, Critical issues and current status of vanadium alloys for fusion energy applications, J. Nucl. Mater. 283 (2000) 70–78.
[48] A.M. Garde, H.M. Chung, T.F. Kassner, Uniaxial Tensile Properties of Zircaloy Containing Oxygen: Summary Report, Argonne National Lab., Ill.(USA), 1977.
[49] J.R. Theaker, R. Choubey, G.D. Moan, S.A. Aldridge, L. Davis, R.A. Graham, C.E. Coleman, Zircon Nucl Int Tenth Int Symp, Fabrication of Zr-2.5 Nb pressure tubes to minimize the harmful effects of trace elements, ASTM International, 1994.
[50] G. Vigna, L. Lanzani, G. Domizzi, S.E. Bermudez, J. Ovejero-García, R. Piotrkowski, Effect of carbides on the hydriding and oxidation behavior of a Zr-2.5 Nb alloy, J. Nucl. Mater. 218 (1995) 18–29.
[51] R.A. Ploc, Residual carbon impurities in Zr–2.5 Nb and their effect on deuterium pickup, J. Nucl. Mater. 279 (2000) 344–350.
[52] M.R. Gilbert, T. Eade, T. Rey, R. Vale, C. Bachmann, U. Fischer, N.P. Taylor, Waste implications from minor impurities in European DEMO materials, Nucl. Fusion 59 (2019) 76015.
[53] C.E. Ells, Hydride precipitates in zirconium alloys (A review), J. Nucl. Mater. 28 (1968) 129–151.
[54] S. Suman, M.K. Khan, M. Pathak, R.N. Singh, J.K. Chakravartty, Hydrogen in Zircaloy: mechanism and its impacts, Int. J. Hydrog.Energy 40 (2015) 5976–5994.
[55] J.W. Davis, M.A. Ulrickson, R.A. Causey, Use of titanium in fusion components, J. Nucl. Mater. 212 (1994) 813–817.
[56] P.L. Andrew, M.A. Pick, Review of tritium retention in first-wall materials, J. Nucl. Mater. 212 (1994) 111–117.
[57] M.A. Tunes, R.W. Harrison, G. Greaves, J.A. Hinks, S.E. Donnelly, Effect of He implantation on the microstructure of zircaloy-4 studied using *in situ* TEM, J. Nucl. Mater. 493 (2017) 230–238.
[58] M.R. Gilbert, S.L. Dudarev, S. Zheng, L.W. Packer, J.C. Sublet, An integrated model for materials in a fusion power plant: transmutation, gas production, and helium embrittlement under neutron irradiation, Nucl. Fusion 52 (2012) 83019.
[59] Q. Zhao, X. Wang, T. Cai, The study of surface properties of ZrO2, Appl. Surf. Sci. 225 (2004) 7–13.
[60] M. Steinbrueck, F.O. da Silva, M. Grosse, Oxidation of Zircaloy-4 in steam-nitrogen mixtures at 600–1200°C, J. Nucl. Mater. 490 (2017) 226–237.
[61] I. Bespalov, M. Datler, S. Buhr, W. Drachsel, G. Rupprechter, Y. Suchorski, Initial stages of oxide formation on the Zr surface at low oxygen pressure: an *in situ* FIM and XPS study, Ultramicroscopy 159 (2015) 147–151.
[62] T. Ahmed, L.H. Keys, The breakaway oxidation of zirconium and its alloys a review, J. Less Common Met. 39 (1975) 99–107.
[63] B. Cox, Adv Corros Sci Technol, in: Oxidation of Zirconium and its Alloys, Springer, 1976, pp. 173–391.
[64] F.J.E.J.S. Leistikow, Zircaloy fuel cladding behavior in a LOCA -a review, in: Proceedings of the Zirconium in the Nuclear Industry Seventh International Symposium, ASTM International, 1985, pp. 24–27.
[65] A.T. Motta, A. Couet, R.J. Comstock, Corrosion of zirconium alloys used for nuclear fuel cladding, Annu. Rev. Mater. Res. 45 (2015) 311–343.
[66] S. Xie, B. Zhou, X. Liang, Q. Li, W. Liu, M. Yao, J. Zhang, The distribution of Li ions in the oxide film formed on zircaloy-4 corroded in lithiated water at 633K, Mater. 13 (2020) 873.
[67] C.W. Bale, The Li– Zr (lithium-zirconium) system, Bull, Alloy Phase Diagr. 8 (1987) 48–50.
[68] M.G. Nicholas, C.F. Old, Liquid metal embrittlement, J. Mater. Sci. 14 (1979) 1–18.
[69] B. Cox, Y.M. Wong, Liquid metal embrittlement of Zr-2.5% Nb alloy, J. Nucl. Mater. 245 (1997) 34–43.
[70] R.F. Koenig, W.A. Heywood, Corrosion of Zirconium and Its Alloys in Liquid Metals, Knolls Atomic Power Laboratory, 1953.
[71] J. Zhang, P. Hosemann, S. Maloy, Models of liquid metal corrosion, J. Nucl. Mater. 404 (2010) 82–96.
[72] K.A. Terrani, Accident tolerant fuel cladding development: promise, status, and challenges, J. Nucl. Mater. 501 (2018) 13–30.
[73] J.C. Brachet, I. Idarraga-Trujillo, M.Le Flem, M.Le Saux, V. Vandenberghe, S. Urvoy, E. Rouesne, T. Guilbert, C. Toffolon-Masclet, M. Tupin, Early studies on Cr-coated zircaloy-4 as enhanced accident tolerant nuclear fuel claddings for light water reactors, J. Nucl. Mater. 517 (2019) 268–285.
[74] L.M. Luo, Y.L. Liu, D.G. Liu, L. Zheng, Y.C. Wu, Preparation technologies and performance studies of tritium permeation barriers for future nuclear fusion reactors, Surf. Coat. Technol. 403 (2020) 126301.
[75] A. Jain, S.P. Ong, G. Hautier, W. Chen, W.D. Richards, S. Dacek, S. Cholia, D. Gunter, D. Skinner, G. Ceder, Commentary: the materials project: a materials genome approach to accelerating materials innovation, APL Mater. 1 (2013) 11002.
[76] R. Gauntt, D. Kalinich, J. Cardoni, J. Phillips, A. Goldmann, S. Pickering, M. Francis, K. Robb, L. Ott, D. Wang, Fukushima daiichi accident study, Sandia Rep. Sand. SAND2012-6173 (2012) 1–297.

[77] (Edited by M. Kuznetsov, J. Grune, A. Friedrich, K. Sempert, W. Breitung, T. Jordan, D. Bradley, G. Makhviladze, V. Molkov, Hydrogen-air deflagrations and detonations in a semi-confined flat layer, in: Proceedings of the Sixth International Seminar on Fire and Explosion Hazards, 2011, pp. 125–136. (Edited by.
[78] L. Baker Jr, Hydrogen-generating Reactions in LWR Severe Accidents, Argonne National Lab., 1983.
[79] J. Yanez, M. Kuznetsov, A. Souto-Iglesias, An analysis of the hydrogen explosion in the Fukushima-daiichi accident, Int. J. Hydrog. Energy 40 (2015) 8261–8280.
[80] B. Kolbasov, C. Barnes, J. Blevins, Plant Systems, ITER, 1991.
[81] B.R. Sehgal, Nuclear Safety in Light Water reactors: Severe Accident Phenomenology, Academic Press, 2011.
[82] M. Lukacs, L.G. Williams, Nuclear safety issues for fusion power plants, Fusion Eng. Des. 150 (2020) 111377.
[83] D. Maisonnier, I. Cook, P. Sardain, R. Andreani, L. Di Pace, R. Forrest, L. Giancarli, S. Hermsmeyer, P. Norajitra, N. Taylor, A conceptual study of commercial fusion power plants. Final report of the european fusion power plant conceptual study (PPCS), EFDA Rep Number EFDA (05)-27/4.10. (2005).
[84] M.E. Sawan, M.A. Abdou, Physics and technology conditions for attaining tritium self-sufficiency for the DT fuel cycle, Fusion Eng. Des. 81 (2006) 1131–1144.
[85] P.K. Romano, N.E. Horelik, B.R. Herman, A.G. Nelson, B. Forget, K. Smith, OpenMC: a state-of-the-art monte carlo code for research and development, in: Proceedings of the SNA + MC 2013 - Joint International Conference on Supercomputing in Nuclear Applications + Monte Carlo, EDP Sciences, 2014, p. 6016.
[86] T. Eade, M. Garcia, R. Garcia, F. Ogando, P. Pereslavtsev, J. Sanz, G. Stankunas, A. Travleev, Activation and decay heat analysis of the European DEMO blanket concepts, Fusion Eng. Des. 124 (2017) 1241–1245.
[87] F. Moro, A. Del Nevo, D. Flammini, E. Martelli, R. Mozzillo, S. Noce, R. Villari, Neutronic analyses in support of the WCLL DEMO design development, Fusion Eng. Des. 136 (2018) 1260–1264.
[88] L.A. El-Guebaly, A. Team, ARIES-ST nuclear analysis and shield design, Fusion Eng. Des. 65 (2003) 263–284.
[89] L. El-Guebaly, L. Mynsberge, A. Davis, C. D'Angelo, A. Rowcliffe, B. Pint, A.-.A. Team, Design and evaluation of nuclear system for ARIES-ACT2 power plant with DCLL blanket, Fusion Sci. Technol. 72 (2017) 17–40.
[90] M.R. Gilbert, M. Fleming, J.C. Sublet, Automated inventory and material science scoping calculations under fission and fusion conditions, Nucl. Eng. Technol. 49 (2017) 1346–1353.
[91] I. Cook, D. Maisonnier, N.P. Taylor, D.J. Ward, P. Sardain, L. Di Pace, L. Giancarli, S. Hermsmeyer, P. Norajitra, R. Forrest, European fusion power plant studies, Fusion Sci. Technol. 47 (2005) 384–392.
[92] M.R. Gilbert, T. Eade, C. Bachmann, U. Fischer, N.P. Taylor, Activation, decay heat, and waste classification studies of the European DEMO concept, Nucl. Fusion. 57 (2017) 46015.
[93] R.E. Melchers, On the ALARP approach to risk management, Reliab. Eng. Syst. Saf. 71 (2001) 201–208.
[94] L.V. Boccaccini, G. Aiello, J. Aubert, C. Bachmann, T. Barrett, A. Del Nevo, D. Demange, L. Forest, F. Hernandez, P. Norajitra, Objectives and status of EURO fusion DEMO blanket studies, Fusion Eng. Des. 109 (2016) 1199–1206.
[95] M. Devillers, M. Sirch, S. Bredendiek-Kämper, R.D. Penzhorn, Characterization of the zirconium-cobalt (ZrCo)-hydrogen system in view of its use for tritium storage, Chem. Mater. 2 (1990) 255–262.
[96] T. Yamanishi, T. Hayashi, Y. Kawamura, Tritium accountancy and storage by hydrogen adsorption alloy in fusion fuel cycle, Seramikkusu 46 (2011) 201–205.
[97] R.G. Budynas, J.K. Nisbett, Shigley's Mechanical Engineering Design, McGraw-Hill New York, 2008.
[98] V. Sears, Neutron scattering lengths and cross sections, Neutron News (1992) 29–37.
[99] E.M. Schulson, D.B. Graham, The effect of transformation temperature on the hardness of the peritectoid phase Zr 3 Al, J. Nucl. Mater. 57 (1975) 358–360.
[100] E.M. Schulson, Zr3Al: a potential nuclear reactor structural material, in: Intermetallic Compounds Principles and Practice, John Wiley Sons Ltd., Hoboken, 1994, pp. 133–146.
[101] E.M. Schulson, J.A. Roy, The notch-sensitivity of ordered Zr3Al, J. Nucl. Mater. 71 (1977) 124–133.
[102] X.J. Jiang, Y.Y. Zhang, C.L. Li, G.D. Liang, R.H. Han, X.Y. Zhang, Microstructure and mechanical properties of ZrAl binary alloys, J. Alloys Compd. 811 (2019) 152068.
[103] E.M. Schulson, J.A. Roy, The yield strength of the L12 phase Zr3Al, Acta Metall. 26 (1978) 29–38.
[104] E.M. Schulson, The tensile and corrosion behaviour of ordered Zr3Al-based alloys, J. Nucl. Mater. 50 (1974) 127–138.
[105] R. Kondo, N. Nomura, Y. Tsutsumi, H. Doi, T. Hanawa, Microstructure and mechanical properties of as-cast Zr–Nb alloys, Acta Biomater. 7 (2011) 4278–4284.
[106] L. Chai, H. Wu, S. Wang, B. Luan, Y. Wu, X. Huang, Microstructural characteristics of cold-rolled Zr-2.5 Nb alloy annealed near the monotectoid temperature, Sci. China Technol. Sci. 61 (2018) 558–566.
[107] M. Griffiths, J.E. Winegar, A. Buyers, The transformation behaviour of the β-phase in Zr–2.5 Nb pressure tubes, J. Nucl. Mater. 383 (2008) 28–33.
[108] Z.N. Yang, X.B. Wang, F. Liu, F.C. Zhang, L.J. Chai, R.S. Qiu, L.Y. Chen, Effect of intercritical annealing temperature on microstructure and mechanical properties of duplex Zr-2.5 Nb alloy, J. Alloys Compd. 776 (2019) 242–249.
[109] B.S. Rodchenkov, A.N. Semenov, High temperature mechanical behavior of Zr–2.5% Nb alloy, Nucl. Eng. Des. 235 (2005) 2009–2018.
[110] G.J.C. Carpenter, E.F. Ibrahim, J.F. Watters, The aging response of zirconium-tin alloys, J. Nucl. Mater. 102 (1981) 280–291.
[111] D. Arias, L. Roberti, The solubility of tin in α and β zirconium below 1000 C, J. Nucl. Mater. 118 (1983) 143–149.
[112] S.L. Wadekar, S. Banerjee, V.V. Raman, M.K. Asundi, Correlation of microstructure and mechanical properties of Zr-Sn alloys, in: Proceedings of the Zirconium in the Nuclear Industry International Symposium, ASTM International, 1991.
[113] Z.H. Feng, C.Q. Xia, R. Jing, X.J. Jiang, Y.K. Zhou, H. Zhong, X.Y. Zhang, M.Z. Ma, R.P. Liu, Microstructure and mechanical properties of ZrBe alloys processed by hot rolling, Mater. Sci. Eng. A 667 (2016) 286–292.
[114] Z.H. Feng, C.Q. Xia, X.J. Jiang, S.G. Liu, X. Zhang, X.Y. Zhang, M.Z. Ma, R.P. Liu, Investigating the structure-property correlation of a novel Zirconium alloy by annealing treatment, Mater. Sci. Eng. A 677 (2016) 393–399.
[115] H.C. Hsu, S.C. Wu, S.K. Hsu, Y.C. Sung, W.F. Ho, Effects of heat treatments on the structure and mechanical properties of Zr–30Ti alloys, Mater. Charact. 62 (2011) 157–163.
[116] S. Banerjee, R. Krishnan, Martensitic transformation in Zr− Ti alloys, Metall. Trans. 4 (1973) 1811–1819.
[117] H.C. Hsu, S.C. Wu, Y.C. Sung, W.F. Ho, The structure and mechanical properties of as-cast Zr–Ti alloys, J. Alloys Compd. 488 (2009) 279–283.
[118] Z.G. Zhang, Y.K. Zhou, X.J. Jiang, Z.H. Feng, C.Q. Xia, X.Y. Zhang, M.Z. Ma, R.P. Liu, A novel Zr-based alloy microstructure with high strength and excellent ductility, Mater. Sci. Eng. A 651 (2016) 370–375.
[119] Z.G. Zhang, Z.H. Feng, X.J. Jiang, X.Y. Zhang, M.Z. Ma, R.P. Liu, Microstructure and tensile properties of novel Zr–Cr binary alloys processed by hot rolling, Mater. Sci. Eng. A 652 (2016) 77–83.
[120] C. Li, Y. Zhan, W. Jiang, Zr-Si biomaterials with high strength and low elastic modulus, Mater. Des. 32 (2011) 4598–4602.
[121] M.Le Flem, J. Canel, S. Urvoy, Processing and characterization of Zr3Si2 for nuclear applications, J. Alloys Compd. 465 (2008) 269–273.
[122] N. Nomura, K. Oya, Y. Tanaka, R. Kondo, H. Doi, Y. Tsutsumi, T. Hanawa, Microstructure and magnetic susceptibility of as-cast Zr–Mo alloys, Acta Biomater. 6 (2010) 1033–1038.
[123] A.V. Nikulina, V.F. Konkov, M.M. Peregud, E.E. Vorobev, Effect of molybdenum on properties of zirconium components of nuclear reactor core, Nucl. Mater. Energy 14 (2018) 8–13.
[124] H.C. Dong, Z.H. Feng, M.Z. Ma, X.Y. Zhang, R.P. Liu, Optimization of phase composition and mechanical properties in Zr alloys by micro-alloying, Mater. Lett. 202 (2017) 25–27.
[125] H. Ren, X. Liu, J. Ning, Microstructure and mechanical properties of W-Zr reactive materials, Mater. Sci. Eng. A 660 (2016) 205–212.
[126] D. Araki, K. Kurosaki, H. Kimura, H. Muta, Y. Ohishi, K. Konashi, S. Yamanaka, Thermal and mechanical properties of hydrides of Zr–Hf alloys, J. Nucl. Sci. Technol. 52 (2015) 162–170.
[127] N.I. Taluts, A.V. Dobromyslov, Structural and phase transformations in quenched and aged Zr–Os alloys, J. Alloys Compd. 298 (2000) 181–189.
[128] N.I. Taluts, A.V. Dobromyslov, V.A. Elkin, Structural and phase transformations in quenched and aged Zr–Ru alloys, J. Alloys Compd. 282 (1999) 187–196.
[129] A.V. Dobromyslov, N.I. Taluts, The formation of α double-prime-phase in Zr-Re alloys, Scr. Mater. 35 (1996) 573–577.
[130] J.Q. Peng, Y. Chen, G.Q. Yan, M. Wu, L.J. Wang, J.S. Li, Solid solubility extension and microstructure evolution of cast zirconium yttrium alloy, Rare Met. 35 (2016) 325–330.
[131] E. Fischer, C. Colinet, An updated thermodynamic modeling of the Al-Zr system, J. Phase Equilib. Diffus. 36 (2015) 404–413.
[132] I. Baker, E.M. Schulson, On grain boundaries in nickel-rich Ni3Al, Scr. Metall. 23 (1989) 1883–1886.
[133] H.E. Rosinger, The effect of neutron irradiation on the tensile properties and growth of zirconium-8.6 wt% aluminum, At. Energy Can. Ltd. (1976).
[134] E.M. Schulson, G.J.C. Carpenter, L.M. Howe, Irradiation swelling of Zr3Al, J. Nucl. Mater. 82 (1979) 140–147.
[135] L.M. Howe, M.H. Rainville, A study of the irradiation behaviour of Zr3Al, J. Nucl. Mater. 68 (1977) 215–234, doi:10.1016/0022-3115(77)90241-0.
[136] J.H. Li, Q. Li, F.C. Zhang, S. Liu, L. Mao, B.C. Hu, Z.N. Yang, Effects boron on microstructure and mechanical properties of Zr3Al-based alloys, Mater. Lett. 153 (2015) 70–72.
[137] E.M. Schulson, D.J. Cameron, Preparation of Zirconium Alloys, U.S. Patent No. 4,094,706, Washington, DC: U.S. Patent and Trademark Office., 1978.
[138] P. Fernández, A.M. Lancha, J. Lapeña, R. Lindau, M. Rieth, M. Schirra, Creep strength of reduced activation ferritic/martensitic steel Eurofer'97, Fusion Eng. Des. 75 (2005) 1003–1008.
[139] C.S. Seok, B. Marple, Y.J. Song, S. Gollapudi, I. Charit, K.L. Murty, High temperature deformation characteristics of Zirlo™ tubing via ring-creep and burst tests, Nucl. Eng. Des. 241 (2011) 599–602.
[140] R.S.W. Shewfelt, L.W. Lyall, D.P. Godin, A high-temperature creep model for Zr-2.5 wt% Nb pressure tubes, J. Nucl. Mater. 125 (1984) 228–235.
[141] B. Cox, Oxidation of Zirconium-Aluminum alloys Atomic Energy of Canada Ltd, Chalk River, Ontario (Canada), 1967.
[142] E.V. Murphy, R. Wieler, The corrosion behaviour of Zr 3 Al-based alloys, At. Energy Can. Ltd. (1977).

[143] J. Ejenstam, Corrosion Resistant Alumina-Forming Alloys For Lead-Cooled Reactors (PhD thesis), KTH Royal Institute of Technology, 2015.
[144] M. Paljević, Z. Ban, Oxidation of stoichiometric Zr3Al-based alloy, J. Nucl. Mater. 95 (1980) 253–258.
[145] B.A. Cheadle, C.E. Coleman, H. Licht, CANDU-PHW pressure tubes: their manufacture, inspection, and properties, Nucl. Technol. 57 (1982) 413–425.
[146] S.B. Farina, A.G. Sanchez, S. Ceré, Effect of surface modification on the corrosion resistance of Zr-2.5 Nb as material for permanent implants, Proc. Mater. Sci. 8 (2015) 1166–1173.
[147] B.S. Hickman, The formation of omega phase in titanium and zirconium alloys: a review, J. Mater. Sci. 4 (1969) 554–563.
[148] T. Tokunaga, S. Matsumoto, H. Ohtani, M. Hasebe, Thermodynamic analysis of the phase equilibria in the Nb-Ni-Zr system, Mater. Trans. 48 (2007) 2263–2271.
[149] J.P. Mardon, D. Charquet, J. Senevat, Influence of composition and fabrication process on out-of-pile and in-pile properties of M5 alloy, in: Proceedings of the Zirconium Nuclear Industry Twelfth International Symposium, ASTM International, 2000.
[150] A. Stern, J.C. Brachet, V. Maillot, D. Hamon, F. Barcelo, S. Poissonnet, A. Pineau, J.P. Mardon, A. Lesbros, Investigations of the microstructure and mechanical properties of prior-β structure as a function of the oxygen content in two zirconium alloys, J. ASTM Int. 5 (2008) 1–20.
[151] B. Cazalis, J. Desquines, C. Poussard, M. Petit, Y. Monerie, C. Bernaudat, P. Yvon, X. Averty, The PROMETRA program: fuel cladding mechanical behavior under high strain rate, Nucl. Technol. 157 (2007) 215–229.
[152] J. Wei, P. Frankel, E. Polatidis, M. Blat, A. Ambard, R.J. Comstock, L. Hallstadius, D. Hudson, G.D.W. Smith, C.R.M. Grovenor, The effect of Sn on autoclave corrosion performance and corrosion mechanisms in Zr–Sn–Nb alloys, Acta Mater. 61 (2013) 4200–4214.
[153] R.J. Pérez, C. Toffolon-Masclet, J.M. Joubert, B. Sundman, The Zr–Sn binary system: new experimental results and thermodynamic assessment, Calphad. 32 (2008) 593–601.
[154] S.Y. Lee, K.T. Kim, S.I. Hong, Circumferential creep properties of stress-relieved zircaloy-4 and Zr–Nb–Sn–Fe cladding tubes, J. Nucl. Mater. 392 (2009) 63–69.
[155] M.J. Rubel, V. Bailescu, J.P. Coad, T. Hirai, J. Likonen, J. Linke, C.P. Lungu, G.F. Matthews, L. Pedrick, V. Riccardo, Beryllium plasma-facing components for the ITER-Like Wall Project at JET, J. Phys. Conf. Ser. 100 (100) (2008) 62028.
[156] Y. Mishima, N. Yoshida, H. Takahashi, K. Ishida, H. Kawamura, T. Iwadachi, T. Shibayama, I. Ohnuma, Y. Sato, K. Munakata, Present status of beryllides for fusion and industrial applications in Japan, Fusion Eng. Des. 82 (2007) 91–97.
[157] T. Tokunaga, H. Ohtani, M. Hasebe, Thermodynamic analysis of the Zr–Be system using thermochemical properties based on ab initio calculations, Calphad 30 (2006) 201–208.
[158] L.E. Tanner, R. Ray, Metallic glass formation and properties in Zr and Ti alloyed with Be—I the binary Zr-Be and Ti-Be systems, Acta Metall. 27 (1979) 1727–1747.
[159] K.C.H. Kumar, P. Wollants, L. Delacy, Thermodynamic assessment of the Ti- Zr system and calculation of the Nb- Ti- Zr phase diagram, J. Alloys Compd. 206 (1994) 121–127.
[160] S.L. Sass, The structure and decomposition of Zr and Ti bcc solid solutions, J. Less Common Met. 28 (1972) 157–173.
[161] W. Cui, Y. Liu, Fatigue behavior of Ti50Zr alloy for dental implant application, J. Alloys Compd. 793 (2019) 212–219.
[162] Y.K. Zhou, S.X. Liang, R. Jing, X.J. Jiang, M.Z. Ma, C.L. Tan, R.P. Liu, Microstructure and tensile properties of hot-rolled Zr50–Ti50 binary alloy, Mater. Sci. Eng. A 621 (2015) 259–264.
[163] H. Okamoto, Cr-Zr (chromium-zirconium), J. Phase Equilibria. 14 (1993) 768.
[164] C.T. Liu, J.H. Zhu, M.P. Brady, C.G. McKamey, L.M. Pike, Physical metallurgy and mechanical properties of transition-metal Laves phase alloys, Intermetallics 8 (2000) 1119–1129, doi:10.1016/S0966-9795(00)00109-6.
[165] M. Griffiths, A review of microstructure evolution in zirconium alloys during irradiation, J. Nucl. Mater. 159 (1988) 190–218.
[166] J.J. Petrovic, A.K. Vasudevan, Key developments in high temperature structural silicides, Mater. Sci. Eng. A 261 (1999) 1–5.
[167] H.M. Chen, Y. Xiang, S. Wang, F. Zheng, L.B. Liu, Z.P. Jin, Thermodynamic assessment of the C–Si–Zr system, J. Alloys Compd. 474 (2009) 76–80.
[168] C. Ramachandra, V. Singh, P.R. Rao, On silicides in high temperature titanium alloys, Def. Sci. J. 36 (1986) 207–220.
[169] P. Barberis, N. Dupin, C. Lemaignan, A. Pasturel, J.M. Grange, Microstructure and Phase Control in Zr-Fe-Cr-Ni alloys: Thermodynamic and Kinetic Aspects, in: Proceedings of the Zirconium Nuclear Industry Twelfth International Symposium, ASTM International, 2005.
[170] H. Zou, G.M. Hood, J.A. Roy, R.J. Schultz, Formation and stability of Fe-rich precipitates in dilute Zr (Fe) single-crystal alloys, Metall. Mater. Trans. A 25 (1994) 1359–1365.
[171] C.-S. Zhang, B. Li, P.R. Norton, The segregation of Fe to a zirconium surface, J. Nucl. Mater. 223 (1995) 238–244.
[172] Y. de Carlan, C. Regnard, M. Griffiths, D. Gilbon, C. Lemaignan, Influence of Iron in the Nucleation of⟨ c⟩ Component Dislocation Loops in Irradiated Zircaloy-4, ASTM International, 1996 Zircon Nucl Ind Eleventh Int Symp.
[173] Z. Karoutas, J. Brown, A. Atwood, L. Hallstadius, E. Lahoda, S. Ray, J. Bradfute, The maturing of nuclear fuel: past to Accident Tolerant Fuel, Prog. Nucl. Energy 102 (2018) 68–78.
[174] H. Okamoto, Mo-Zr (molybdenum-zirconium), J. Phase Equilib. Diffus. 25 (2004) 485.
[175] D.O. Northwood, Heat treatment, transformation reactions and mechanical properties of two high strength zirconium alloys, J. Less Common Met. 61 (1978) 199–212.
[176] C. Servant, Thermodynamic assessments of the phase diagrams of the hafnium-vanadium and vanadium-zirconium systems, J. Phase Equilib. Diffus. 26 (2005) 39–49.
[177] S.K. Lee, D.N. Lee, Calculation of phase diagrams using partial phase diagram data, Calphad 10 (1986) 61–76.
[178] N. Nomura, Y. Tanaka, R. Kondo, H. Doi, Y. Tsutsumi, T. Hanawa, Effects of phase constitution of Zr-Nb alloys on their magnetic susceptibilities, Mater. Trans. 50 (2009) 2466–2472.
[179] X.J. Jiang, Y.K. Zhou, Z.H. Feng, C.Q. Xia, C.L. Tan, S.X. Liang, X.Y. Zhang, M.Z. Ma, R.P. Liu, Influence of Zr content on β-phase stability in α-type Ti–Al alloys, Mater. Sci. Eng. A 639 (2015) 407–411.
[180] X.J. Jiang, R. Jing, C.Y. Liu, M.Z. Ma, R.P. Liu, Structure and mechanical properties of TiZr binary alloy after Al addition, Mater. Sci. Eng. A 586 (2013) 301–305.
[181] X.J. Jiang, G. Yu, Z.H. Feng, C.Q. Xia, C.L. Tan, X.Y. Zhang, M.Z. Ma, R.P. Liu, Abnormal β-phase stability in TiZrAl alloys, J. Alloys Compd. 699 (2017) 256–261.
[182] C. Veiga, J.P. Davim, A.J.R. Loureiro, Properties and applications of titanium alloys: a brief review, Rev. Adv. Mater. Sci. 32 (2012) 133–148.
[183] R. Jing, S.X. Liang, C.Y. Liu, M.Z. Ma, X.Y. Zhang, R.P. Liu, Structure and mechanical properties of Ti–6Al–4V alloy after zirconium addition, Mater. Sci. Eng. A 552 (2012) 295–300.
[184] S.X. Liang, M.Z. Ma, R. Jing, X.Y. Zhang, R.P. Liu, Microstructure and mechanical properties of hot-rolled ZrTiAlV alloys, Mater. Sci. Eng. A 532 (2012) 1–5.
[185] Y.B. Tan, L.H. Yang, J.L. Duan, L.Y. Ji, W.C. Liu, Studies on the kinetics of $\beta\rightarrow\alpha$ phase transformation in 47Zr–45Ti–5Al–3V alloy under isothermal conditions by X-ray diffraction, Mater. Charact. 112 (2016) 98–104.
[186] S.X. Liang, M.Z. Ma, R. Jing, C.L. Tan, R.P. Liu, Structural evolution and mechanical properties of Zr–45Ti–5Al–3V alloy by heat treatments, Mater. Sci. Eng. A 541 (2012) 67–72.
[187] L. Qu, Z.N. Yang, F.C. Zhang, M. Zhang, X.Y. Zhang, R.P. Liu, Effect of deformation and heat treatment on the microstructure and mechanical properties of β-Zr40Ti5Al4V alloy, J. Alloys Compd. 612 (2014) 80–89.
[188] J. Li, X. Zhang, J. Qin, M. Ma, R. Liu, Strength and grain refinement of Ti-30Zr-5Al-3V alloy by Fe addition, Mater. Sci. Eng. A 691 (2017) 25–30.
[189] S.X. Liang, L.X. Yin, L.Y. Zheng, M.Z. Ma, R.P. Liu, Preparation of low cost TiZrAlFe alloy with ultra-high strength and favorable ductility, Mater. Sci. Eng. A 639 (2015) 699–704.
[190] M.J.R. Barboza, C.M. Neto, C.R.M. Silva, Creep mechanisms and physical modeling for Ti–6Al–4V, Mater. Sci. Eng. A 369 (2004) 201–209.
[191] L. Badea, M. Surand, J. Ruau, B. Viguier, Creep Behavior of Ti-6Al-4V from 450°C to 600°C, University Polytechnica of Bucharest Sci Bulletin. Series B 76 (2014) 185–196.
[192] G. Lütjering, J.C. Williams, A. Gysler, Microstructure and mechanical properties of titanium alloys, Microstruct. Prop. Mater. 2 (2000) 1–77.
[193] L. Nie, Y. Zhan, T. Hu, X. Chen, C. Wang, Novel high-strength ternary Zr–Al–Sn alloys with martensite structure for nuclear applications, J. Nucl. Mater. 442 (2013) 100–105.
[194] L. Nie, Y. Zhan, H. Liu, C. Tang, Novel β-type Zr–Mo–Ti alloys for biological hard tissue replacements, Mater. Des. 53 (2014) 8–12.
[195] L. Nie, Y. Zhan, T. Hu, X. Chen, C. Wang, β-Type Zr–Nb–Ti biomedical materials with high plasticity and low modulus for hard tissue replacements, J. Mech. Behav. Biomed. Mater. 29 (2014) 1–6.
[196] P. Chui, Near β-type Zr-Nb-Ti biomedical alloys with high strength and low modulus, Vacuum 143 (2017) 54–58.
[197] S.J. Zinkle, J.L. Boutard, D.T. Hoelzer, A. Kimura, R. Lindau, G.R. Odette, M. Rieth, L. Tan, H. Tanigawa, Development of next generation tempered and ODS reduced activation ferritic/martensitic steels for fusion energy applications, Nucl. Fusion 57 (2017) 92005.
[198] D.J.M. King, S.C. Middleburgh, A.G. McGregor, M.B. Cortie, Predicting the formation and stability of single phase high-entropy alloys, Acta Mater. 104 (2016) 172–179, doi:10.1016/j.actamat.2015.11.040.
[199] J. Yeh, S. Chen, S. Lin, J. Gan, T. Chin, T. Shun, C. Tsau, S. Chang, Nanostructured high-entropy alloys with multiple principal elements: novel alloy design concepts and outcomes, Adv. Eng. Mater. 6 (5) (2004) 299–303.
[200] B. Cantor, I. Chang, P. Knight, A. Vincent, Microstructural development in equiatomic multicomponent alloys, Mater. Sci. Eng. A (2004) 213–218.
[201] D.B. Miracle, O.N. Senkov, A critical review of high entropy alloys and related concepts, Acta Mater. 122 (2017) 448–511.
[202] Y. Zhou, Y. Zhang, Y. Wang, G. Chen, Microstructure and compressive properties of multicomponent Alx(TiVCrMnFeCoNiCu)100-x high-entropy alloys, Mater. Sci. Eng. A 454 (2007) 260–265.
[203] B.S. Li, Y.P. Wang, M.X. Ren, C. Yang, H.Z. Fu, Effects of Mn, Ti and V on the microstructure and properties of AlCrFeCoNiCu high entropy alloy, Mater. Sci. Eng. A 498 (2008) 482–486.
[204] Y.L. Chen, Y.H. Hu, C.A. Hsieh, J.W. Yeh, S.K. Chen, Competition between elements during mechanical alloying in an octonary multi-principal-element alloy system, J. Alloys Compd. 481 (2009) 768–775.
[205] Z. Wang, S. Guo, C.T. Liu, Phase selection in high-entropy alloys: from nonequilibrium to equilibrium, JOM 66 (2014) 1966–1972, doi:10.1007/s11837-014-0953-8.

[206] S. Gorsse, M.H. Nguyen, O.N. Senkov, D.B. Miracle, Database on the mechanical properties of high entropy alloys and complex concentrated alloys, Data Br. 21 (2018) 2664–2678.
[207] O.N. Senkov, D.B. Miracle, K.J. Chaput, J.P. Couzinie, Development and exploration of refractory high entropy alloys—a review, J. Mater. Res. 33 (19) (2018) 1–37.
[208] K. Jin, C. Lu, L.M. Wang, J. Qu, W.J. Weber, Y. Zhang, H. Bei, Effects of compositional complexity on the ion-irradiation induced swelling and hardening in Ni-containing equiatomic alloys, Scr. Mater. 119 (2016) 65–70.
[209] O. El-Atwani, N. Li, M. Li, A. Devaraj, J.K.S. Baldwin, M.M. Schneider, D. Sobieraj, J.S. Wróbel, D. Nguyen-Manh, S.A. Maloy, Outstanding radiation resistance of tungsten-based high-entropy alloys, Sci. Adv. 5 (2019) eaav2002.
[210] D.J.M. King, S.T.Y. Cheung, S.A. Humphry-Baker, C. Parkin, A. Couet, M.B. Cortie, G.R. Lumpkin, S.C. Middleburgh, A.J. Knowles, High temperature, low neutron cross-section high-entropy alloys in the Nb-Ti-V-Zr system, Acta Mater. 166 (2019) 435–446, doi:10.1016/j.actamat.2019.01.006.